fire

MDPI

Article

Study on Smoke Control Strategies for Tunnel Fires Under Near-Critical Velocity Conditions

Xiaokun Zhao [1,2], Yafei Tian [1,2,*], Xiangzhong Zhang [1,2], Anyu Song [1,2], Wencai Wang [3] and Donghui Yang [1,2]

[1] School of Coal Engineering, Shanxi Datong University, Datong 037000, China; zhaoxiaokun@sxdtdx.edu.cn (X.Z.); 240857002144@sxdtdx.edu.cn (X.Z.); 240857002148@sxdtdx.edu.cn (A.S.); 18306828103@163.com (D.Y.)
[2] Cultivation Base of Shanxi Key Laboratory of Coal Mine Water Jet Technology and Equipment, Datong 037003, China
[3] School of Mining and Coal, Inner Mongolia University of Science and Technology, Baotou 014010, China; 19834450184@163.com
* Correspondence: 240857002105@sxdtdx.edu.cn

Abstract

High-temperature toxic smoke from tunnel fires poses a serious threat to safe evacuation, while direct experimental support is still lacking for the performance transition and parameter matching resulting from the combined action of centralized smoke extraction and a water curtain under near-critical longitudinal ventilation. To investigate their combined smoke control performance under near-critical longitudinal ventilation, this study combines FDS numerical simulations, 1:10 reduced-scale experiments, and dimensionless analysis to examine the effects of the smoke extraction rate and water curtain parameters on temperature and CO concentration in an 8 MW tunnel fire. The results show that, without a water curtain, 15 m^3/s is a representative suitable smoke extraction rate among the discrete cases; with 500 μm droplets and a flow rate of 40 L/min per nozzle, the 18 m^3/s case exhibits comparatively favorable smoke control performance after the water curtain is introduced. As the flow rate per nozzle increases from 30 to 60 L/min, the smoke extraction performance transition interval shifts from 17–18 to 20–21 m^3/s, and a dimensionless interval-constrained relation is established: $\Pi_e = 3.90596\Pi_w + 0.32834$. This relation applies to the fixed geometry, fire, ventilation, and spray conditions in this study and is not for direct use in engineering design.

Keywords: tunnel fire; centralized smoke extraction; water curtain system; reduced-scale experiment; dimensionless analysis

Check for updates

Academic Editor: Kaihua Lu

Received: 22 September 2026
Revised: 27 October 2026
Accepted: 30 October 2026
Published: 5 November 2026

Copyright: © 2026 by the authors. Licensee MDPI, Basel, Switzerland. This article is an open access article distributed under the terms and conditions of the Creative Commons Attribution (CC BY) license.

1. Introduction

With the continued development of road transport infrastructure, the number of tunnels and the scale of their construction continue to increase. Because tunnels are long, narrow, and relatively enclosed, with limited evacuation exits and weak natural ventilation, high-temperature toxic smoke generated by vehicle fires can rapidly accumulate and spread longitudinally along the tunnel, reducing visibility, increasing temperature, and raising the concentrations of toxic gases such as CO, thereby seriously threatening the safety of evacuation and firefighting and rescue operations [1,2]. Therefore, maintaining tenable conditions at evacuation height while limiting smoke backlayering and longitudinal spread is a central issue in research on tunnel fire ventilation, smoke extraction, and smoke control.

Existing research on tunnel fire smoke control mainly concerns longitudinal ventilation, centralized smoke extraction, and water-based smoke control systems, with experimental

studies providing an important basis for understanding the behavior and parameter effects of different smoke control methods. For longitudinal ventilation, Oka and Atkinson [3] revealed a piecewise relationship between critical velocity and fire heat release rate through reduced-scale model experiments, establishing a basis for engineering applications of critical velocity. For centralized smoke extraction, Liu et al. [4] used 1:20 reduced-scale fire experiments to investigate the combined effects of exhaust vent area, width, and smoke extraction rate, finding that different performance indicators responded differently to the extraction rate and vent geometry; Ingason and Li [5] compared the smoke control performance of single-point and two-point extraction systems through 1:23 reduced-scale model experiments, further demonstrating that the number and arrangement of exhaust vents significantly affect smoke control. For water-based smoke control, Chen [6] analyzed the cooling and smoke control effects of a sidewall water spray system at different longitudinal velocities through reduced-scale tunnel fire experiments; Zhu et al. [7] further examined the effects of nozzle pressure, installation position, and longitudinal velocity on the thermal insulation performance of high-pressure water mist, showing pronounced coupling between water mist parameters and ventilation conditions. These experimental results show that longitudinal ventilation, centralized smoke extraction, and water-based smoke control all have clear smoke control effects, but their performance is affected by fire size, system parameters, and spatial arrangement.

Numerical simulations and theoretical studies have further revealed the internal flow mechanisms and parameter responses of different smoke control systems. For longitudinal ventilation, Li et al. [8] established a quantitative relationship between critical velocity and smoke backlayering length and analyzed the physical meanings of the Froude and Richardson numbers in the competition between buoyancy and inertia; Li et al. [9] investigated changes in the maximum ceiling smoke temperature under longitudinal ventilation, showing that longitudinal airflow affects both the extent of smoke backlayering and the downstream smoke layer temperature and stratification stability. Chen et al. [10] used large eddy simulation to investigate the critical velocity in cross-passages of large railway tunnels, further showing that classical critical velocity relations have specific applicability limits under complex structural and blockage conditions.

For centralized smoke extraction, the research focus has gradually shifted from examining the extraction rate alone to the coupling among extraction rate, exhaust vent geometry, fire conditions, and makeup air conditions. Tanaka et al. [11] investigated changes in smoke layer height under combined longitudinal ventilation and point extraction, and Chen et al. [12] combined reduced-scale experiments, FDS simulations, and theoretical analysis to study smoke layer propagation under combined longitudinal ventilation and centralized extraction. Wang et al. [13] conducted a numerical study of plug-holing in centralized extraction under two-fire conditions, showing that fire spacing and extraction parameters jointly affect critical plug-holing conditions. Li et al. [14] found that both the smoke extraction mode and the longitudinal air supply ratio significantly affect smoke spread distance and extraction efficiency; Liu et al. [15] showed that tunnel width, the transverse fire position, and its relative distance from the exhaust vent affect effective heat removal; Shi et al. [16] further demonstrated pronounced coupling between the smoke extraction rate and the number of exhaust vents. When the suction intensity at an exhaust vent exceeds the stability of the upper smoke layer maintained by buoyancy, the induced airflow may penetrate the smoke layer and entrain the cooler air below, producing plug-holing, which reduces effective smoke extraction and disturbs local smoke stratification. Therefore, centralized smoke extraction performance does not improve continuously as the extraction rate increases, and suitable operating conditions require a combined assessment of smoke temperature, pollutant concentration, and the local flow field.

For water-based smoke control and coupling among multiple systems, numerical and theoretical studies further show that droplet size, flow rate, and momentum exchange all alter the smoke layer structure. Wang et al. [17] showed that increasing the water spray flow rate increases droplet-induced drag on smoke, thereby changing smoke layer thickness and stratification stability; Nishino et al. [18] found through large eddy simulation that droplet size significantly affects the continuity and smoke-blocking effect of a water mist barrier; the review by Farrell et al. [19] showed that water mist system performance is affected by the fire scenario, spatial arrangement, spray parameters, and interactions with other fire protection systems. For coupling among multiple systems, Yuan Jianping [20] proposed combining a water curtain with a nearby centralized exhaust vent to form a local smoke control region; Yao et al. [21] investigated the coupling between longitudinal ventilation and natural exhaust shafts, finding that longitudinal airflow changes both smoke extraction capacity and the spatial distribution of smoke. These studies show that different smoke control measures are not simply additive: longitudinal ventilation can suppress upstream smoke backlayering but may enhance downstream smoke transport; centralized extraction can reduce smoke accumulation, but excessive extraction rates may induce cool air entrainment and plug-holing; water curtains can provide cooling, smoke blocking, and thermal insulation, but droplets may also disturb the smoke layer. Thus, when multiple smoke control systems operate together, their parameters interact and require matching.

Existing studies leave three specific questions unresolved. First, under near-critical longitudinal ventilation, over what discrete range of smoke extraction rates do the macroscopic smoke control indicators of centralized extraction shift from improvement to no longer improving together? Second, after a water curtain is introduced, how does this performance transition interval shift with the water curtain flow rate? Third, under fixed fire, geometry, and spray conditions, how can this matching relationship be expressed using dimensionless parameters? To address these questions, this study combines 1:10 reduced-scale experiments with FDS simulations, identifies performance transitions using temperature, CO, local flow fields, and species transport, compares representative cases with and without a water curtain, and establishes an in-sample constraint relation between the water curtain momentum parameter and the smoke extraction transition interval. The contribution of this study is multi-indicator evidence and an interval expression under these controlled conditions; the results do not serve as a universal plug-holing criterion or an engineering design formula.

2. Materials and Methods

2.1. Theoretical Basis and Similarity Criteria

2.1.1. Physical Mechanisms of Coupled Smoke Control by Multiple Systems

As tunnel fire smoke propagates longitudinally, thermal buoyancy, longitudinal airflow inertia, and ceiling exhaust suction jointly affect smoke layer thickness and interface stability. Increasing the centralized smoke extraction rate can improve smoke removal; with a further increase in suction, the air below may penetrate the local smoke layer and enter the exhaust vent, producing plug-holing, whose physical mechanism is shown in Figure 1. Plug-holing describes the local penetration of the smoke layer, whereas the performance transition interval in this study describes the combined response of macroscopic indicators such as temperature and CO to discrete changes in the smoke extraction rate. The two have different concepts and assessment bases.

After a water curtain is introduced, evaporative droplet cooling can reduce smoke temperature and increase its density, while droplet momentum and gas–liquid drag redistribute the local smoke layer, changing the thickness, composition, and entrainment paths of the smoke layer presented to the exhaust vent. Therefore, centralized smoke extraction and

water curtains are not simply additive; their matching relationship fundamentally depends on the competition among thermal buoyancy, longitudinal momentum, suction inertia, and droplet momentum.

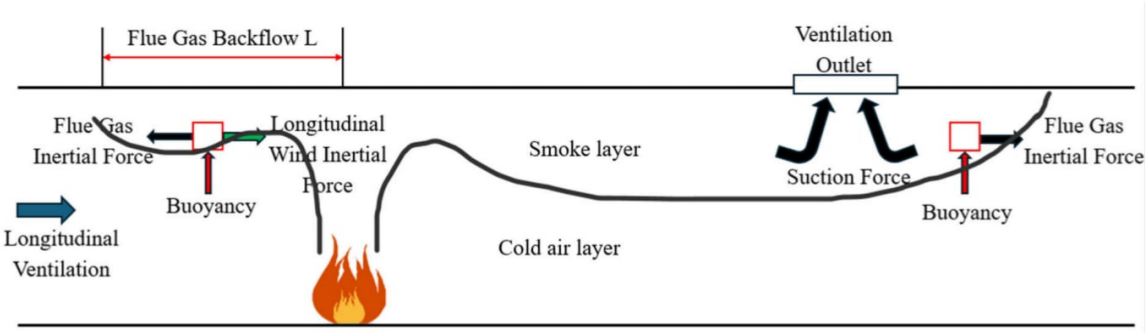


Figure 1. Schematic of longitudinal smoke transport and local plug-holing at the exhaust vent.

2.1.2. Froude Similarity Criteria and Dimensionless Analysis Framework

To establish the scale relationship between the 100 m prototype numerical model and the 1:10 reduced-scale experiments, Froude similarity is adopted for gas-phase fire and ventilation processes [5,6]. With the geometric scale ratio defined as $\lambda_L = L_m/L_p = 0.1$, velocity and heat release rate satisfy $V_m/V_p = \lambda_L{}^{1/2}$ and $Q_m/Q_p = \lambda_L{}^{5/2}$, respectively. Thus, an 8 MW prototype fire corresponds to a reduced-scale fire of approximately 25.3 kW, and a longitudinal velocity of 2.0 m/s corresponds to approximately 0.63 m/s. The prototype time window of 300–600 s corresponds to approximately 94.9–189.7 s in the model under time scaling, while the actual start and end of the statistical period are determined from measured records showing that combustion and the monitored quantities have reached a quasi-steady state.

The total water curtain flow rate is converted to the model design value using the geometric scale ratio raised to the power of 5/2 according to Froude similarity and is then distributed according to the number of model nozzles. In the experiments, nozzle selection and water supply pressure adjustment bring the measured flow rate close to the design value, while the spray angle, characteristic droplet size, and near-nozzle velocity are measured. Achieving the design flow rate does not imply complete similarity of the other spray characteristics. The same-scale FDS model therefore uses the measured flow rate and spray characteristics to set the water curtain boundary and examines the macroscopic response under that reduced-scale condition. The limits of cross-scale water curtain similarity are discussed in Section 4.4.

To reduce the influence of the unit system on the expression of parameter relationships, this study uses the dimensionless extraction intensity Π_e and water curtain momentum parameter Π_w to describe the relative effects of centralized smoke extraction and the water curtain. Π_e represents the extraction suction velocity relative to the gravitational velocity scale, and Π_w represents water curtain momentum relative to the gas-phase gravitational scale. Their definitions are given in Section 2.7.3, and the sample relationship is presented in Section 3.3.

2.2. Design and Implementation of Reduced-Scale Experiments

A 1:10 reduced-scale tunnel fire platform is established according to the Froude similarity relationships in Section 2.1.2 to examine the macroscopic response of coupled centralized smoke extraction and a water curtain. The prototype-to-model relationships for the geometry, fire, and ventilation parameters are listed in Table 1, with a target model heat release rate of 25.3 kW and a target longitudinal velocity of 0.63 m/s.

Table 1. Main parameter relationships between the prototype and the 1:10 reduced-scale model.

Parameter	Prototype	1:10 Model	Scaling Relationship
Tunnel dimensions	100 × 4 × 3 m	10 × 0.40 × 0.30 m	$\lambda_L = 0.1$
Fire location	25 m	2.50 m	λ_L
Fire footprint	4 × 2 m	0.40 × 0.20 m	λ_L
Exhaust vent	2 × 4 m	0.20 × 0.40 m	λ_L
Water curtain–exhaust vent distance	8 m	0.80 m	λ_L
Heat release rate	8 MW	25.3 kW	$\lambda_L^{5/2}$
Longitudinal velocity	2.0 m/s	0.63 m/s	$\lambda_L^{1/2}$

The reduced-scale platform consists of the tunnel structure, longitudinal ventilation, fire source, centralized smoke extraction, water curtain, and data acquisition systems. An n-heptane pool fire is used as the model fire source, and the actual heat release rate is estimated from the fuel mass loss rate to establish a same-scale FDS model with matching boundary conditions. The apparatus and design parameters are listed in Table 2.

Table 2. Reduced-scale experimental apparatus and main design parameters.

Experimental System	Main Equipment	Design Parameters and Requirements
Tunnel structure	Steel frame, fire-resistant asbestos mesh, and transparent observation windows	10 m × 0.40 m × 0.30 m
Longitudinal ventilation	Variable-frequency axial fan and YHD2 ventilation multiparameter detector	Target velocity: 0.63 m/s
Fire source system	n-Heptane fuel, burning pan, and electronic balance	Target HRR: 25.3 kW, calibrated using the mass loss rate
Centralized smoke extraction	Exhaust fan and exhaust ducting	Exhaust vent: 0.20 m × 0.40 m; smoke extraction rate: approximately 114–285 m^3/h
Water curtain system	Pressure-adjustable water supply pump and water mist system	Three nozzles directed vertically downward, 0.80 m downstream of the exhaust vent
Temperature measurement	K-type thermocouples and data acquisition instrument	Measurement points along the ceiling and at representative heights
CO concentration measurement	CO gas monitor and sensors	At a height of 0.16 m and at the exhaust vent measurement section

To ensure reliable measurements in the reduced-scale experiments, the measurement systems for temperature, CO concentration, longitudinal velocity, smoke extraction rate, water curtain flow rate, spray pressure, and fuel mass were calibrated before testing. The temperature measurement system underwent multipoint calibration using a standard temperature source, the CO analyzer underwent zero and span calibration using standard gases of known concentrations, and the velocity and flow measurement devices were checked against corresponding standard devices or independent measurement methods. The accuracies reported in this study are the permissible errors specified in instrument manuals or calibration certificates; instrument resolution is treated separately from measurement accuracy.

The reduced-scale experimental apparatus is shown in Figures 2–7:

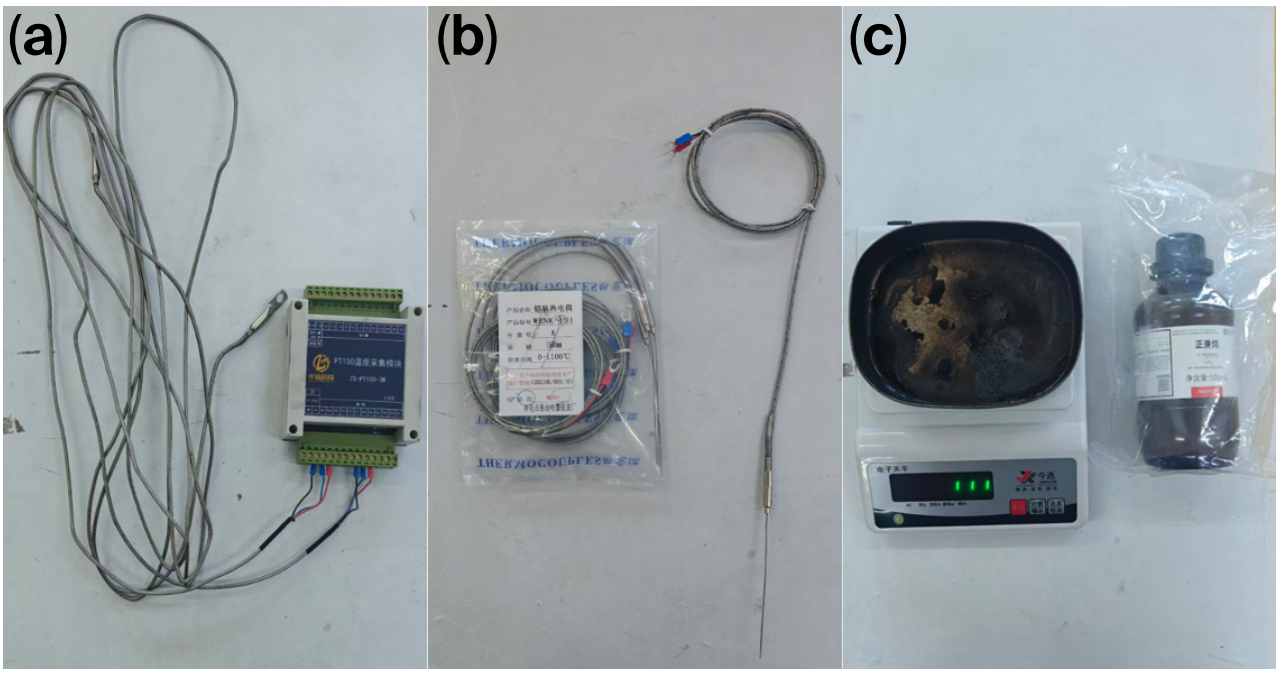


Figure 2. Fire source system and temperature measurement apparatus. (**a**) Temperature acquisition module; (**b**) sheathed thermocouple; (**c**) electronic balance and n-heptane fuel.



Figure 3. Water curtain system. (**a**) Pressure-adjustable water supply pump; (**b**) water mist system.

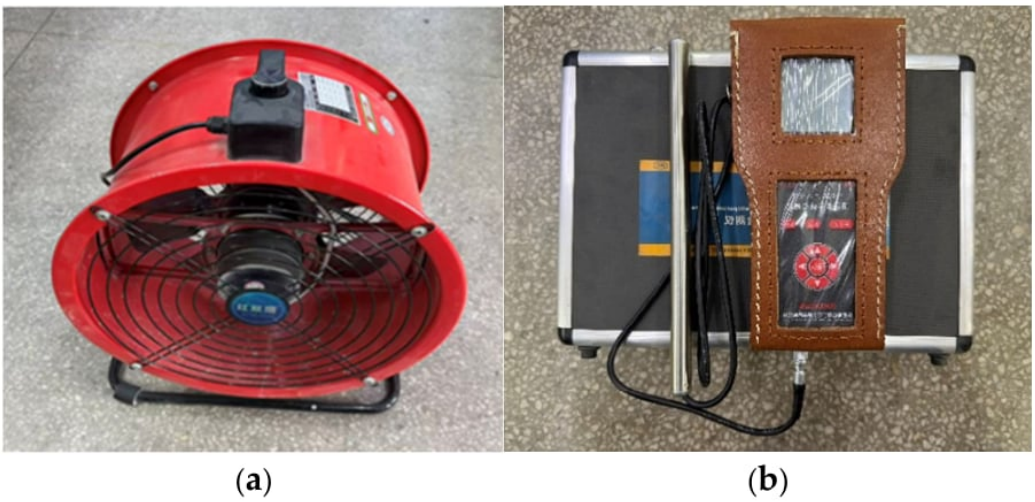


Figure 4. Longitudinal ventilation system. (**a**) Variable-frequency axial fan; (**b**) YHD2 ventilation multiparameter detector.



Figure 5. Exhaust fan and exhaust ducting.

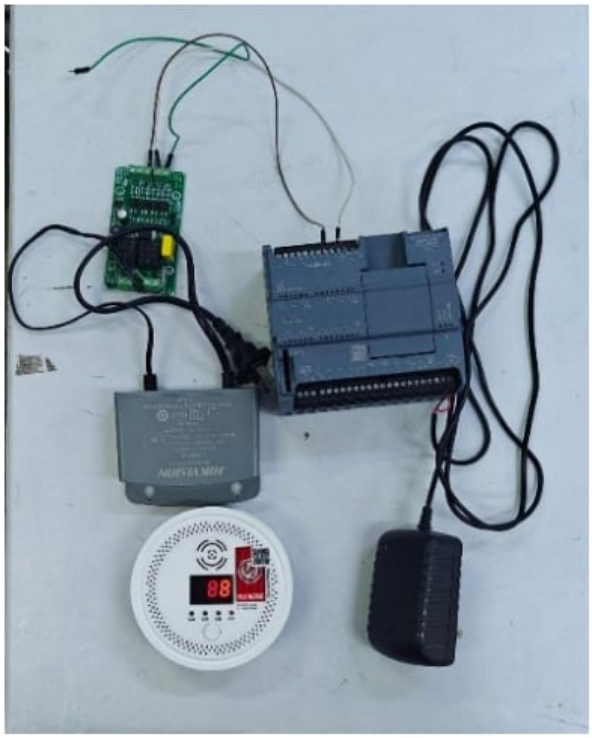


Figure 6. CO monitor and sensors.

The reduced-scale validation scheme includes cases without a water curtain and cases with coupled water curtain operation. Prototype-equivalent smoke extraction rates of 10, 15, 20, and 25 m^3/s are selected without a water curtain, and rates of 15, 18, 20, and 25 m^3/s are selected with a water curtain. Each case is converted using the Froude volumetric flow scaling relationship; the design values are listed in Table 3.



Figure 7. Reduced-scale experimental platform.

Table 3. Reduced-scale experimental cases.

Case	Water Curtain	Prototype-Equivalent Extraction Rate/(m^3/s)	Model Extraction Rate/(m^3/s)	Main Purpose
E1	Absent	10	0.0316	Low-extraction baseline
E2	Absent	15	0.0474	Favorable numerical case
E3	Absent	20	0.0632	Performance transition
E4	Absent	25	0.0791	High extraction/cool air entrainment
E5	Present	15	0.0474	Water curtain introduction baseline
E6	Present	18	0.0569	Representative coupled case
E7	Present	20	0.0632	Coupled transition
E8	Present	25	0.0791	Strong suction disturbance

During testing, a stable longitudinal airflow is first established, after which the fire is ignited and smoke extraction and the water curtain are activated according to a consistent sequence; temperature, CO concentration, and operating parameters are recorded during the quasi-steady stage. The prototype evacuation height of 1.6 m corresponds to 0.16 m in the model. Each case is repeated three times. The tabulated results are means of the repeated experiments, with repeatability error characterized by the standard deviation or coefficient of variation. Combined measurement uncertainty accounts for instrument accuracy, calibration error, and repeated-measurement fluctuations.

2.3. FDS Model and Boundary Conditions

This study establishes a prototype-scale FDS domain of 100 m × 4 m × 3 m, with the fire located 25 m from the upstream entrance, a ceiling exhaust vent of 2 m × 4 m, and a water curtain 8 m downstream of the vent [22–30]. The Oka–Atkinson critical velocity

relation is used to determine the longitudinal ventilation boundary. For an 8 MW fire and a tunnel height of H = 3 m, the theoretical critical velocity is V_c = 1.90 m/s. The longitudinal velocity at the upstream inlet is therefore set to 2.0 m/s, corresponding to V/V_c = 1.05, to represent longitudinal ventilation close to and slightly above the theoretical critical value; this value serves as the common ventilation boundary in this study and is not a new critical velocity prediction. An OPEN boundary is set at the downstream end, and the tunnel walls are adiabatic. A 4.0 m × 2.0 m rectangular burner represents the 8 MW n-heptane fire. The HRR grows according to a t^2 law, reaches 8 MW at approximately 206.5 s, and then remains constant; CO and soot yields are set to 0.006 and 0.015 kg/kg, respectively, as shown in Figure 8. For the 1:10 reduced-scale experiments, a same-scale FDS validation model of 10 m × 0.40 m × 0.30 m is also established. Its geometry, fire conditions, longitudinal velocity, smoke extraction rate, and spray inputs match the actual reduced-scale experimental parameters to compare the macroscopic response of the coupling process with the experiments.

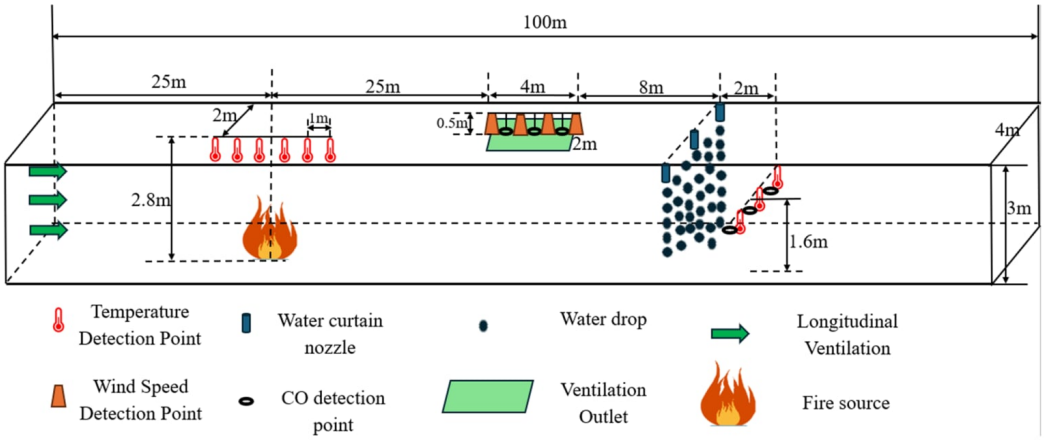


Figure 8. Schematic of the prototype-scale apparatus and monitoring positions.

Water Curtain and Droplet Model

The water curtain consists of three nozzles uniformly arranged across the tunnel width and directed vertically downward (Table 4). The reference pressure is 0.4 MPa (4 bar), and the flow coefficient is K = 20 L·min^{-1}·bar$^{-1/2}$. Using q = K$\sqrt{P}$ gives a baseline flow rate of 40 L/min per nozzle and a total flow rate of 120 L/min for the three nozzles. Throughout this paper, p denotes the flow rate per nozzle, and the total water curtain flow rate is 3p. In the variable-flow cases, flow rate is an independent numerical parameter, while the volume median droplet diameter, initial velocity, distribution, and spray angle remain unchanged; these cases therefore do not represent the pressure-dependent performance curve of an actual nozzle. The volume median droplet diameter is 500 μm, the Rosin–Rammler/lognormal distribution parameters are γ = 2.4 and σ = 0.6, and the inner and outer angles of the solid cone are 0° and 30°. PARTICLE_VELOCITY is set directly to 5 m/s; this value is neither calculated from 0.4 MPa nor measured experimentally. The computational particle release rate is 2000 s^{-1}·nozzle^{-1}, and sensitivity analysis examines its effect on time-averaged macroscopic indicators.

The water curtain system investigated in this study is a numerical model established to analyze interactions between water droplets and tunnel fire smoke, rather than an engineering design for a particular tunnel automatic sprinkler system. The water-based system represents a vertically downward water curtain for smoke control and does not simulate fire extinction or suppression of the fire source. The common geometry, fire, ventilation, spray,

and statistical settings are listed together in Section 2 and the case tables. The parameters varied across cases are specified in Section 2.6.

Table 4. Baseline parameters of the numerical water curtain model.

Parameter	Setting	Description
Number of nozzles	3	Uniformly arranged across the tunnel width
Spray direction	Vertically downward	Fixed
Water curtain position	8 m downstream of the exhaust vent	Fixed arrangement in this study
Volume median droplet diameter	500 μm	Selected representative droplet size
Baseline flow rate per nozzle	40 L/min/nozzle (total flow rate of three nozzles: 120 L/min)	FDS input setting
Spray pattern	Solid cone	FDS input setting
Spray angle	30°	FDS input setting
Droplet size distribution	Rosin–Rammler/lognormal	$\gamma = 2.4$; $\sigma = 0.6$
Initial droplet velocity	5 m/s	Numerical input parameter
Computational droplet release rate	2000 s^{-1}·$nozzle^{-1}$	See particle release rate sensitivity analysis
Reference operating pressure	0.4 MPa	Baseline point for the 40 L/min nozzle only
Flow coefficient	K = 20 L·min^{-1}·$bar^{-1/2}$	$q = K\sqrt{P}$

2.4. Mesh and Numerical Sensitivity

This study uses Fire Dynamics Simulator (FDS 6.7.9), developed by the US National Institute of Standards and Technology (NIST), to calculate smoke transport in tunnel fires. The characteristic fire diameter D^* characterizes the fire plume scale, and the computational mesh is selected in conjunction with mesh sensitivity results. D^* is defined as follows [31]:

$$D^* = \left(\frac{Q}{\rho_0 c_p T_0 \sqrt{g}} \right)^{2/5} \quad (1)$$

In Equation (1), D^* is the characteristic fire diameter, m; Q is the heat release rate, kW; ρ_∞ is the air density, taken as 1.205 kg/m^3; c_p is the specific heat of air at constant pressure, taken as 1.003 kJ/(kg·K); T_0 is the initial ambient temperature, taken as 293 K (20 °C); g is the gravitational acceleration, taken as 9.81 m/s^2; and x is the mesh size, taken as 0.10–0.30 m.

2.4.1. Global Mesh and Temporal Stability

To examine the effect of mesh size on macroscopic outputs, a gas temperature monitoring point is placed near the ceiling 5 m from the fire, and the temperature responses of five mesh sizes, 0.10, 0.15, 0.20, 0.25, and 0.30 m, are compared during the quasi-steady stage of 300–600 s (Figure 9). This indicator is the gas temperature near the ceiling rather than the solid wall temperature.

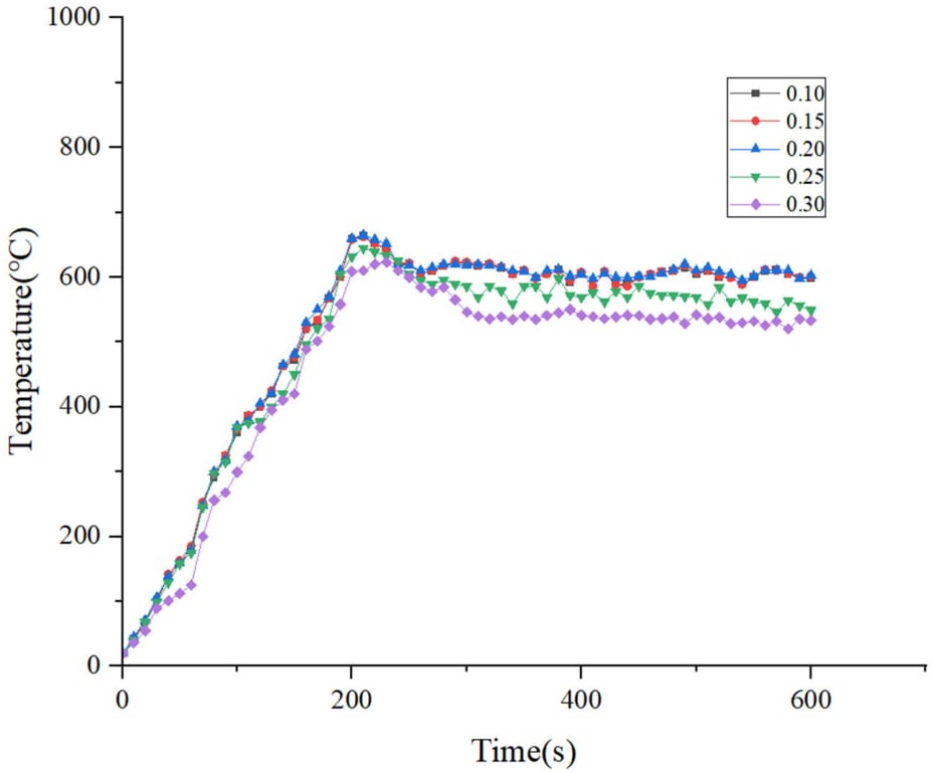


Figure 9. Near-ceiling gas temperature responses for different mesh sizes.

Calculated using Equation (1) and the listed thermophysical properties, D* for the 8 MW fire is approximately 2.20 m; for a 0.20 m mesh, D*/δx is approximately 11. The computational domain contains 500 × 20 × 15 cells, totaling 150,000 computational cells. Mesh selection is based on the sensitivity results for temperature, CO, and the local time-averaged indicators presented below, rather than treating a particular D*/δx value as a universal guarantee of accuracy. The simulation duration and fire growth settings are given in Section 2.3; Table 5 examines the temporal stability of the 300–600 s statistical window using the 15 m^3/s case.

Table 5. Temporal stability check of the quasi-steady statistical window.

Monitored Parameter	Mean over 300–450 s	Mean over 450–600 s	Mean over 300–600 s	Relative Difference Between Subintervals
Ceiling temperature/°C	536.8	527.3	532.1	1.80%
CO concentration at the exhaust vent section/ppm	1123.6	1103.2	1113.4	1.80%
Mean CO concentration at 1.6 m height/ppm	32.4	31.2	31.8	3.77%

The example results show differences of 1.80–3.77% between the two subintervals, with differences between the subinterval means of all key parameters below 5%. Therefore, 300–600 s is selected as the quasi-steady stage for statistical analysis.

To further examine the effect of mesh size on smoke transport results, the CO concentration at the exhaust vent section is selected as an additional assessment indicator. The figure presents the temporal variation in exhaust vent CO concentration for mesh sizes of 0.10, 0.15, 0.20, 0.25, and 0.30 m. The results for different mesh sizes exhibit consistent fire development trends and enter a quasi-steady stage after 300 s (see Table 6).

Table 6. Exhaust vent CO concentrations for different mesh sizes.

Time/s	0.10 m/ppm	0.15 m/ppm	0.20 m/ppm	0.25 m/ppm	0.30 m/ppm
0	0	0	0	0	0
50	6	5	5	4	3
100	35	33	32	28	25
150	180	175	170	155	145
200	620	610	600	570	540
250	1030	1025	1020	980	930
300	1120	1118	1115	1085	1051
350	1132	1130	1128	1100	1070
400	1140	1137	1138	1108	1080
450	1117	1115	1113	1094	1065
500	1110	1108	1105	1084	1050
550	1106	1104	1100	1078	1040
600	1102	1099	1094	1067	1046

With the 0.10 m mesh as the reference, the relative differences in time-averaged exhaust vent CO for the 0.15 and 0.20 m meshes are 0.21% and 0.43%, respectively, and those for the 0.25 and 0.30 m meshes are 2.70% and 5.38%, respectively (Table 7). A 0.20 m mesh is selected accordingly, and Section 2.4.2 further examines the sensitivity of the local time-averaged longitudinal velocity and exhaust vent CO using a representative coupled case.

Table 7. Comparison of time-averaged exhaust vent CO concentrations for different meshes.

Mesh Size/m	Mean CO Concentration over 300–600 s/ppm	Difference Relative to the 0.10 m Mesh/%
0.10	1118.2	-
0.15	1115.9	0.21
0.20	1113.4	0.43
0.25	1088.0	2.70
0.30	1058.0	5.38

2.4.2. Mesh Sensitivity of the Local Flow Field

A representative coupled case with the baseline water curtain conditions in Table 4 and a smoke extraction rate of 18 m^3/s is selected to compare the local mean longitudinal velocity and exhaust vent CO concentration for 0.10, 0.15, and 0.20 m meshes. All indicators use the 300–600 s statistical window specified in Section 2.4.1; the results are listed in Table 8.

Table 8. Local mesh sensitivity for the representative coupled case.

Mesh Size/m	Local Mean Longitudinal Velocity/($m \cdot s^{-1}$)	Exhaust Vent CO Concentration/ppm
0.10	4.72	1441
0.15	4.69	1437
0.20	4.65	1433

Compared with the 0.10 m mesh, the relative differences in local mean longitudinal velocity and exhaust vent CO for the 0.20 m mesh are both within approximately 1.5% (Table 8), indicating that these time-averaged indicators in this representative case are relatively insensitive to further mesh refinement. A 0.20 m mesh is used in subsequent calculations.

2.4.3. Computational Particle Release Rate Sensitivity

The water curtain system in this study describes heat transfer, momentum exchange, and smoke blocking between droplets and high-temperature smoke, rather than the fire-extinguishing action of an actual automatic sprinkler system.

Under the baseline water curtain conditions in Table 4 and a smoke extraction rate of 18 m^3/s, three computational particle release rates of 1000, 2000, and 4000 particles·s^{-1}·$nozzle^{-1}$ are compared. The assessment indicators are the 300–600 s means of temperature and CO concentration at 1.6 m height, maximum ceiling temperature, and exhaust vent CO (Table 9). When the release rate increases from 2000 to 4000 particles·s^{-1}·$nozzle^{-1}$, the relative changes in all indicators remain within approximately 3.2%; therefore, 2000 particles·s^{-1}·$nozzle^{-1}$ is used subsequently.

Table 9. Computational particle release rate sensitivity.

Release Rate/(s^{-1}·$Nozzle^{-1}$)	Mean Temperature at 1.6 m Height/°C	Mean CO at 1.6 m Height/ppm	Maximum Ceiling Temperature/°C	Exhaust Vent CO/ppm
1000	54.3	20.8	556.1	1418
2000	53.0	20.0	542.8	1433
4000	51.6	19.7	537.9	1439

2.5. Numerical Model Validation

2.5.1. Validation of the Longitudinal Ventilation Boundary

This section checks the longitudinal ventilation boundary used; the complete prototype geometry, fire, smoke extraction, and water curtain settings are given in Section 2.3. The definition of dimensionless heat release rate and the piecewise critical velocity correlation are given in Equations (2) and (3), respectively.

The dimensionless heat release rate is defined as follows:

$$Q^* = \frac{Q}{\rho_a \cdot C_p \cdot T_a \cdot \sqrt{g} \cdot H^{5/2}} \tag{2}$$

The corresponding classical piecewise critical velocity relation is [3,32]:

$$V_c = \begin{cases} 0.35\left(\frac{Q^*}{0.124}\right)^{\frac{1}{3}}\sqrt{gH} \cdots Q^* < 0.124 \\ 0.35\sqrt{gH} \cdots Q^* \geq 0.124 \end{cases} \tag{3}$$

In Equations (2) and (3), $g = 9.81\ m/s^2$, $\rho_\infty = 1.2\ kg/m^3$, $c_p = 1005\ J/(kg{\cdot}K)$, $T_0 = 293\ K$, and $H = 3\ m$. Substitution into Equation (3) gives $V_c = 1.90\ m/s$. Thus, the 2.0 m/s used subsequently is a specified longitudinal velocity above the correlation estimate rather than the theoretical critical velocity itself.

Figure 10 shows pronounced upstream smoke backlayering at lower longitudinal velocities. When the longitudinal velocity increases to 2.0 m/s, persistent upstream backlayering is markedly suppressed; with a further increase in longitudinal velocity, smoke is still transported mainly downstream. This trend agrees with the calculated theoretical critical velocity of $V_c = 1.90\ m/s$, indicating that 2.0 m/s can serve as the near-critical longitudinal ventilation boundary for the 8 MW fire and 4 m × 3 m tunnel cross-section investigated in this study.



Figure 10. Upstream smoke propagation at different longitudinal velocities.

2.5.2. Baseline Validation Against Existing Full-Scale Experiments

To assess the ability of the FDS model to predict the smoke temperature field in a longitudinally ventilated tunnel fire, the full-scale tunnel fire experiment T2-2 conducted by Zhu et al. [7] is selected for validation within a limited scope. The experimental tunnel measures 20 m × 5 m × 5 m, the fire source is a 2 m × 2 m n-heptane pool fire, the quasi-steady mean heat release rate is 4.9 MW, and the longitudinal ventilation velocity is 2.1 m/s. The validation model follows the experimental geometry, wall thermophysical properties, fire size, and ventilation conditions. Eleven temperature measurement points are placed 0.05 m below the tunnel ceiling, and temperatures are time-averaged over the quasi-steady period of 100–200 s. The experimental temperature data are digitized from Figure 12 of the cited reference (see Table 10).

Table 10. Comparison of the baseline temperature field for the T2-2 full-scale experiment.

Distance from Fire/m	Experimental Temperature/°C	FDS-Predicted Temperature/°C	Absolute Error/°C	Relative Error/%
−10	29	31	2	6.90
−8	30	32	2	6.67
−6	33	35	2	6.06
−4	47	50	3	6.38
−2	76	82	6	7.89
0	115	108	7	6.09
2	120	114	6	5.00
4	108	102	6	5.56
6	91	89	2	2.20
8	84	80	4	4.76
10	79	75	4	5.06

The FDS results generally agree well with the experimental data. For the 11 measurement points, the mean absolute error is 4.00 °C, the root mean square error is 4.41 °C, and the mean absolute percentage error is 5.69%. Relative errors at all measurement points are below 8%, with the maximum relative error of 7.89% occurring 2 m upstream of the fire. The results show that the established FDS model can reasonably predict the longitudinal distribution of tunnel ceiling temperature under longitudinal ventilation.

2.5.3. Comparison Between Reduced-Scale Experiments and Same-Scale FDS Simulations

A same-scale FDS model is established using the actual reduced-scale experimental boundaries in Section 2.2 to compare the longitudinal ceiling temperature distribution, CO concentration at 0.16 m height, and exhaust vent CO. Figures 11–15 examine these macroscopic indicators and their trends with smoke extraction rate; prototype-equivalent experimental extraction rates are converted according to Table 3 and are treated separately from the absolute temperatures or concentrations of the prototype model.

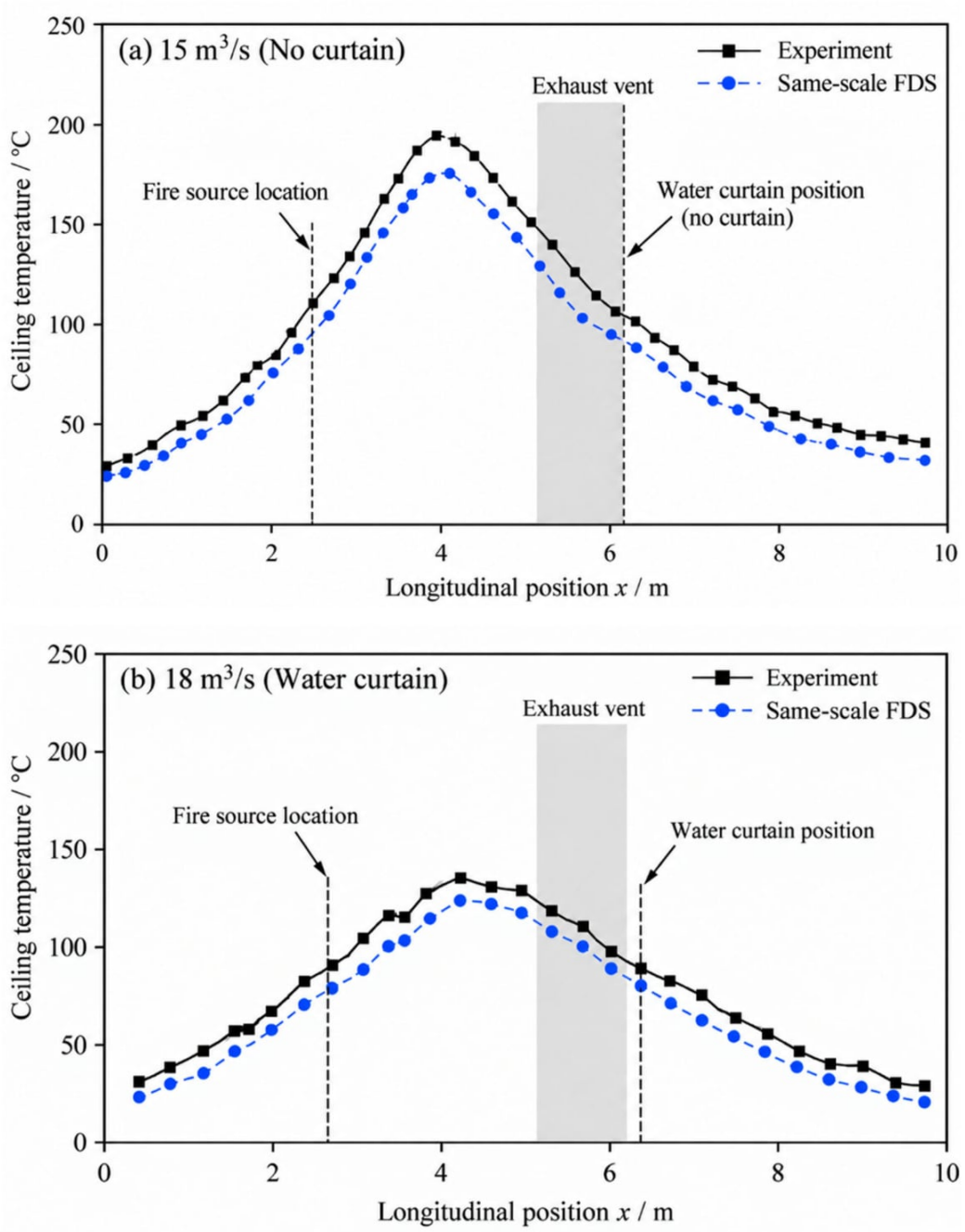


Figure 11. Comparison of longitudinal ceiling temperature distributions between reduced-scale experiments and same-scale FDS simulations. (**a**) Prototype-equivalent extraction rate of 15 m^3/s, without a water curtain. (**b**) Prototype-equivalent extraction rate of 18 m^3/s, with a water curtain.

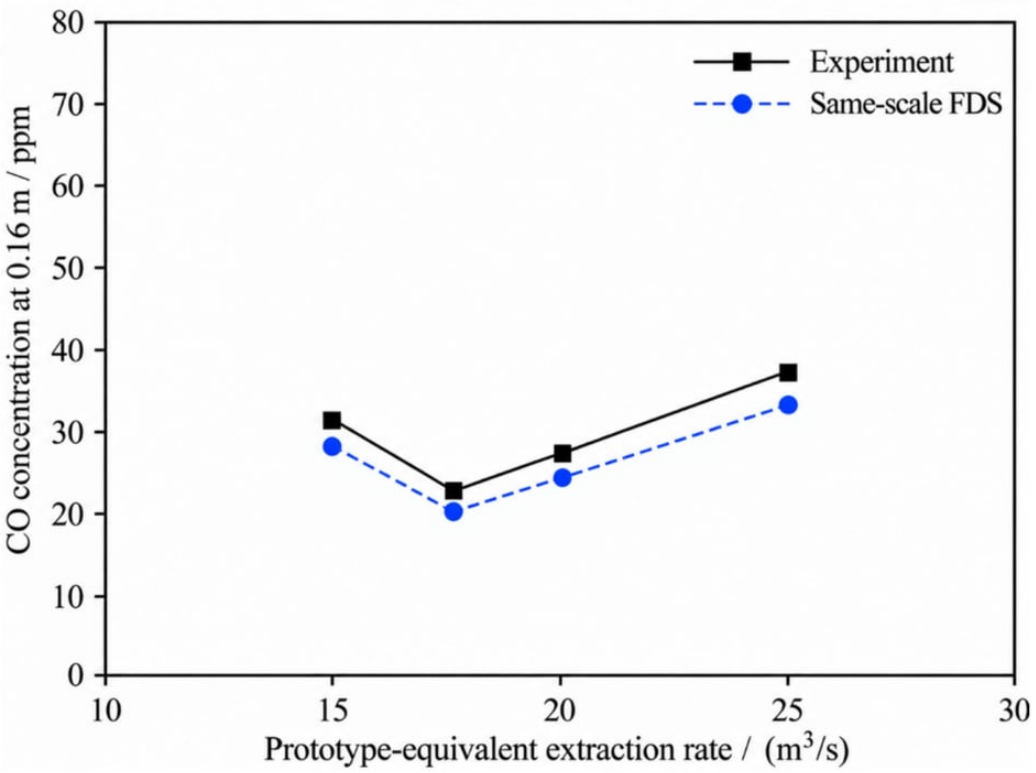


Figure 12. Comparison of CO at 0.16 m height between experiments and same-scale FDS simulations at different prototype-equivalent extraction rates.

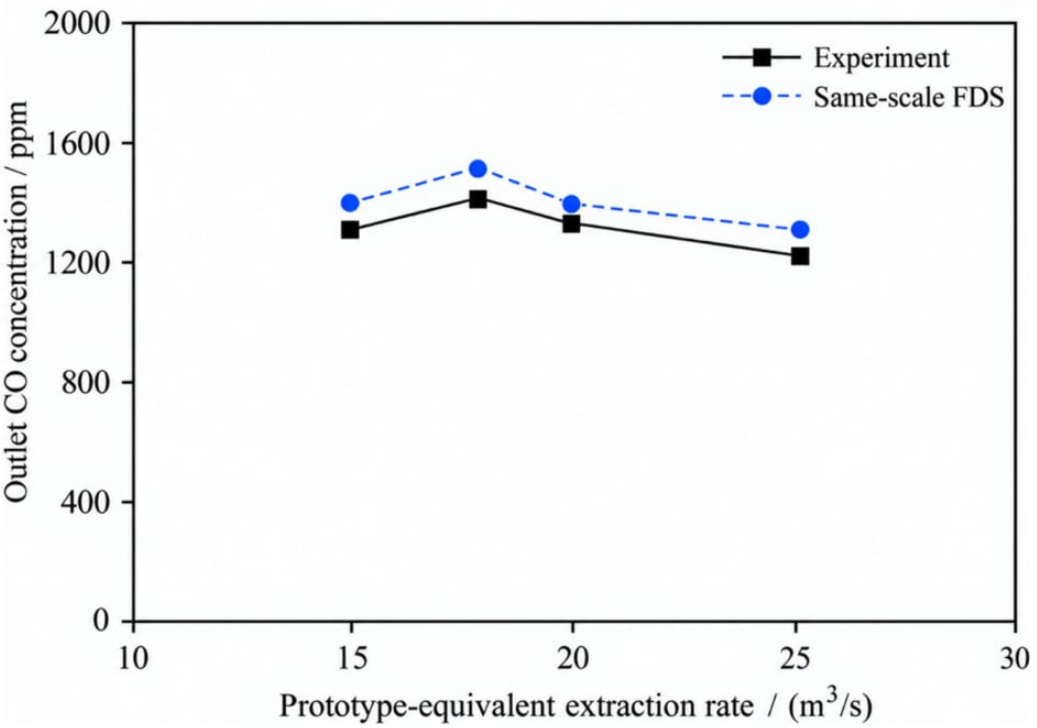


Figure 13. Comparison of exhaust vent CO between experiments and same-scale FDS simulations at different prototype-equivalent extraction rates.

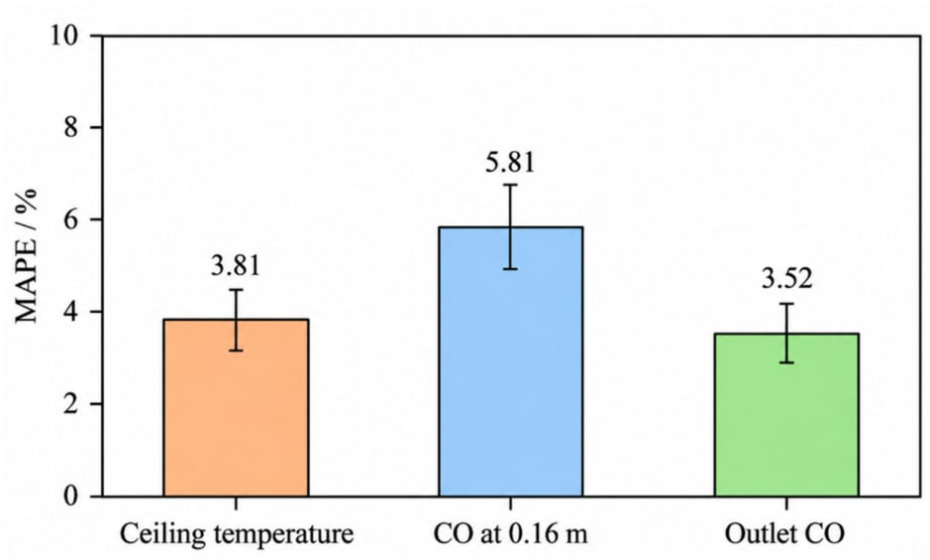


Figure 14. MAPE and standard deviation of APE for same-scale FDS simulations and reduced-scale experiments.

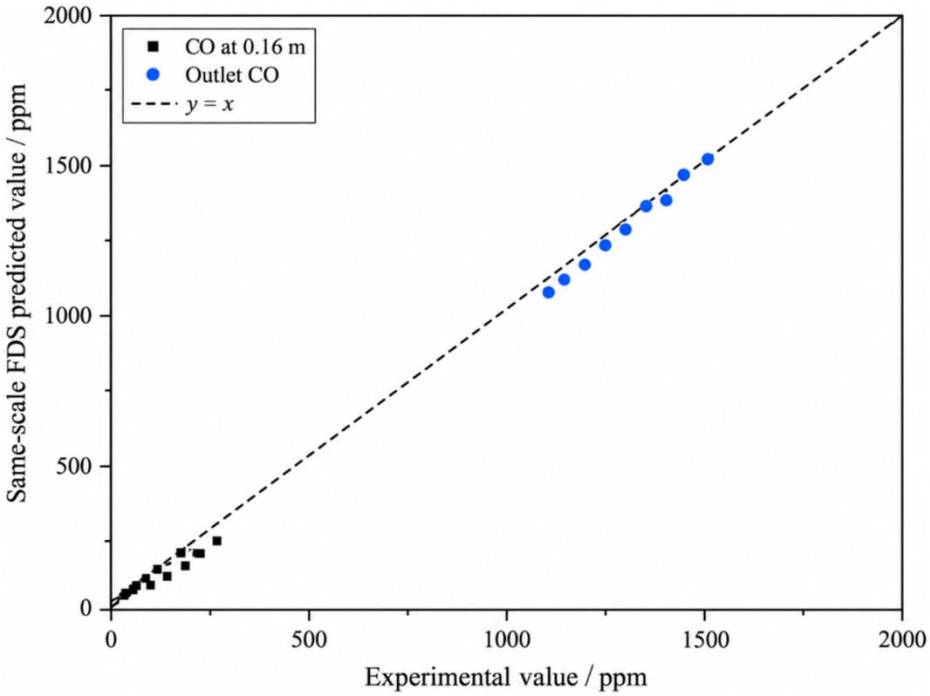


Figure 15. Agreement between experimental and same-scale FDS-predicted CO concentrations.

Figure 14 and Table 11 present the mean absolute percentage error (MAPE) for each set of paired data. Error bars indicate the standard deviation of the paired absolute percentage errors (APEs), rather than the standard deviation of repeated experiments or a confidence interval. The MAPE values for the three indicators are 3.81%, 5.81%, and 3.52%, respectively, showing differences in the model prediction deviations among macroscopic outputs.

Comparisons between the reduced-scale experiments and same-scale FDS simulations for temperature distributions, evacuation-height CO, and exhaust vent CO provide a macroscopic-response basis for subsequent prototype-scale parameter comparisons. Section 3.1 analyzes the baseline without a water curtain, Section 3.2 compares the responses after a water curtain is introduced, and Section 3.3 reports the interval expression from refined extraction rates under fixed conditions.

Table 11. Error statistics for paired same-scale FDS and reduced-scale experimental data.

Validation Indicator	Number of Data Pairs N	MAPE/%	Standard Deviation of APE/%
Ceiling temperature	30	3.81	1.26
CO concentration at 0.16 m height	4	5.81	2.15
Exhaust vent CO concentration	4	3.52	1.08

2.6. Simulation Cases and Monitoring Indicators

2.6.1. Extraction Cases Without a Water Curtain

Under the near-critical longitudinal ventilation boundary specified in Section 2, cases without a water curtain are set at extraction rates of 5–30 m^3/s in increments of 5 m^3/s (Table 12) to analyze changes in temperature, CO, and local transport responses as the extraction rate increases.

Table 12. Cases with progressively increasing extraction rates without a water curtain.

Simulation Number	1	2	3	4	5	6
Extraction Rate (m^3/s)	5	10	15	20	25	30

The operating boundaries and statistical window for all cases follow Section 2. The evacuation-height CO point is 10 m downstream of the exhaust vent and 1.6 m above the floor, while exhaust vent temperature, CO, and local velocity are also monitored. Temperature and CO use different monitoring positions, with between-case comparisons made at the same point for each quantity; the overall monitoring arrangement is shown in Figure 8. The corresponding settings with and without a water curtain are listed in Table 13.

Table 13. Cases comparing extraction rates with a water curtain.

Number	Simulation Type	Water Curtain Parameters	Extraction Rate/m^3/s
1	Control group	No water curtain	15
2	Simulation group 1	Droplet size: 500 μm, Flow rate: 40 L/min	15
3	Simulation group 2	Droplet size: 500 μm, Flow rate: 40 L/min	18
4	Simulation group 3	Droplet size: 500 μm, Flow rate: 40 L/min	20

2.6.2. Droplet Size and Coupled Extraction Cases

The droplet-size comparison includes cases without a water curtain and with droplets of 200, 300, 500, and 800 μm.

In the droplet size cases, the evacuation-height temperature measurement point is 2 m downstream of the water curtain and 1.6 m above the floor; exhaust vent CO and maximum ceiling temperature are also evaluated.

The subsequent coupled cases vary the extraction rate only, using the baseline spray inputs in Table 4 for the water curtain; the corresponding settings with and without a water curtain are listed in Table 13.

The statistical window follows Section 2.4.1; monitoring positions are given in Section 2 and Figure 8.

2.6.3. Cases with Variable Water Curtain Flow Rates

Under the prototype boundaries specified in Section 2 and with 500 μm droplets, the flow rate per nozzle is set to 30, 35, 40, 45, 50, 55, and 60 L/min. Each group uses candidate extraction rates of 15–21 m^3/s in increments of 1 m^3/s.

2.7. Data Processing and Dimensionless Analysis

2.7.1. Identification of Performance Transition Intervals

In this study, a "suitable smoke extraction rate" is defined as a representative operating parameter with comparatively favorable combined macroscopic temperature and CO indicators among a finite set of discrete cases. A "performance transition interval" is the range between adjacent extraction-rate cases over which continuous improvement changes to stabilization, an increase, or a loss of simultaneous improvement among the indicators; exhaust vent CO, local flow fields, and species mass transport provide supporting explanations. This interval depends on the sampling increment, assessment indicators, and apparatus conditions and differs from the precise extraction rate at the onset of plug-holing or a universal plug-holing threshold. The identification procedure is given below.

The CO concentration at 1.6 m height characterizes the relative pollution level at the specified monitoring position and is used with the temperature indicator at the same height to assess macroscopic responses. The horizontal positions of the two indicators follow their respective measurement point definitions, so they represent measurements at different points.

Performance transition intervals are identified from adjacent discrete cases. First, the 300–600 s mean temperature, evacuation-height CO, and exhaust vent CO are compared under the same water curtain input and monitoring positions. Second, adjacent cases are located where increasing the extraction rate changes the macroscopic indicators from improvement to stabilization, an increase, or a loss of simultaneous improvement, with local flow fields and available species transport results providing supporting explanations.

2.7.2. Species Mass Transport Definitions

To further analyze the relationship between this performance transition and cool air entrainment, exhaust vent CO concentration alone provides insufficient information to directly distinguish an increase in nominal extraction rate from changes in the actual removal of high-temperature smoke. Therefore, the total mass flow rate, smoke species mass flow rate, and cool air mass fraction at the exhaust vent section are further extracted for analysis under the same fire and longitudinal ventilation conditions.

To quantitatively assess the transport of combustion products and ambient air during smoke extraction, a virtual mass flux measurement plane matching the exhaust vent area is placed at the vent section. Following the FDS conservation formulation [33], the total mass flow rate is defined as the area integral of the normal mass flux:

$$\dot{m}_{tot} = \int_A \rho u_n dA \tag{4}$$

where A is the exhaust vent area, ρ is the local gas density, and u_n is the gas velocity normal to the exhaust vent section. To characterize the smoke content of the extracted airflow, the combustion product species PRODUCTS in the FDS simple chemistry model is used for analysis [33], with its mass flow rate defined as

$$\dot{m}_{prod} = \int_A \rho u_n Y_{prod} dA \tag{5}$$

where Y_{prod} is the local mass fraction of the combustion product species. Correspondingly, the unreacted air mass flow rate is expressed as

$$\dot{m}_{air} = \int_A \rho u_n Y_{air} dA \tag{6}$$

and the air mass flow fraction in the extracted airflow is defined as

$$\eta_{air} = \frac{\dot{m}_{air}}{\dot{m}_{tot}} \times 100\% \tag{7}$$

Equations (4)–(7) define mass flux post-processing quantities; the FDS species variables are described in Reference [33].

2.7.3. Dimensionless Parameters and Interval-Constrained Analysis

To characterize relative changes in centralized extraction suction and water curtain input consistently, the dimensionless extraction intensity and water curtain momentum parameter are defined, respectively, as

$$\prod_e = \frac{Q_e}{A_e\sqrt{gH}} \tag{8}$$

$$\prod_{\text{w}} = \frac{\rho_{\text{w}} Q_{\text{w}} V_d}{\rho_a g H A_t} \tag{9}$$

where Q_e is the nominal volumetric extraction rate, A_e is the exhaust vent area, and H is the tunnel height; $Q_w = 3p$ is the total water curtain flow rate of the three nozzles, V_d is the initial droplet velocity, A_t is the tunnel cross-sectional area, and ρ_w and ρ_a are the water and air densities, respectively. Π_e characterizes the extraction suction velocity relative to the gravitational velocity scale, and Π_w characterizes water curtain momentum relative to the gas-phase gravitational scale. This study uses $A_e = 8\ m^2$, $H = 3\ m$, $A_t = 12\ m^2$, $V_d = 5\ m/s$, $\rho_w = 1000\ kg/m^3$, and $\rho_a = 1.2\ kg/m^3$. According to Equations (8) and (9), both Q_e and Q_w are first converted to m^3/s, after which the different water curtain flow rates and corresponding extraction transition intervals are converted into dimensionless parameters.

To summarize the trend in the seven discrete intervals, an interval-constrained linear relation is used:

$$\Pi e.fit = a\Pi w + b \tag{10}$$

Let the lower and upper bounds of the ith transition interval be L_i and U_i, respectively. The parameters are determined by maximizing the minimum distance d between the values calculated from the linear relation and the nearest interval boundary: $\max_{a,b,d} d$, subject to $L_i + d \le a\Pi_{w,i} + b \le U_i - d$. The resulting relation is reported in Section 3.3.2.

3. Results

3.1. Performance Transition of Centralized Smoke Extraction Under Near-Critical Longitudinal Ventilation

3.1.1. Temperature Response

When the extraction rate increases from 5 to 15 m^3/s, both the maximum ceiling temperature and the temperature at the 1.6 m measurement point in Table 14 decrease; when the rate increases from 15 to 20 m^3/s, they rise from 608.5 and 34.2 °C to 626.5 and 38.1 °C, respectively. Together with Figure 16, this shows a reversal in the thermal environment improvement trend with a further increase in extraction rate, accompanied by changes in the local smoke layer distribution.

Table 14. Temperature responses at different extraction rates without a water curtain.

Number	Extraction Rate (m^3/s)	Maximum Ceiling Temperature/°C	Mean Temperature 5 m from the Exhaust Vent at 1.6 m Height/°C
1	5	677.6	65.4
2	10	642.9	49.6
3	15	608.5	34.2
4	20	626.5	38.1
5	25	636.9	42.2
6	30	659.2	54.9

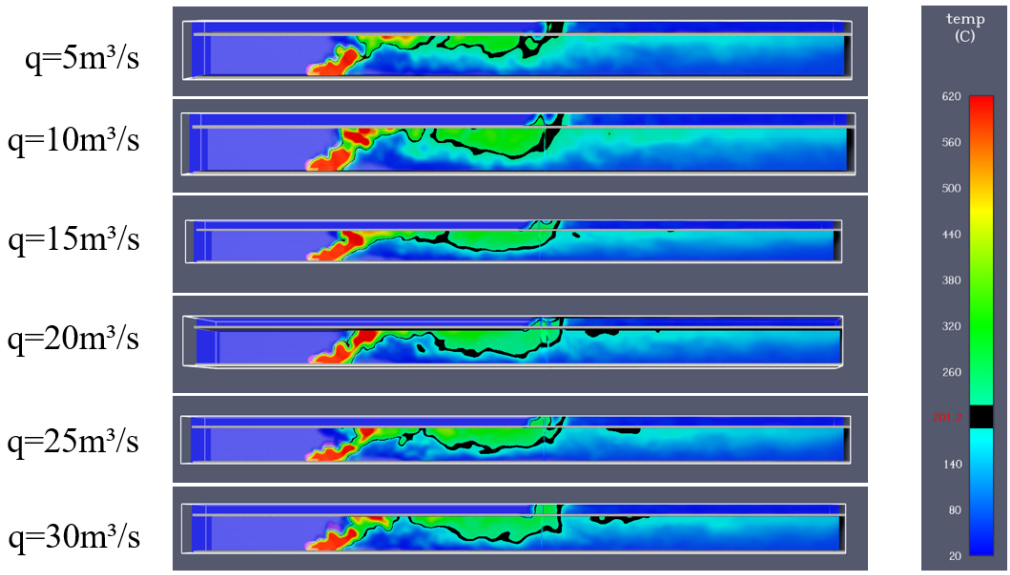


Figure 16. Temperature distributions at different extraction rates without a water curtain.

3.1.2. CO Concentration Response

Table 15 shows that evacuation-height CO first decreases and then increases with extraction rate, reaching 32 ppm in the 15 m^3/s case and increasing to 128 ppm in the 30 m^3/s case. Together with the temperature results, 15 m^3/s is a representative suitable value among the tested cases without a water curtain. Figure 17 gives the CO time history at another monitoring point at the tunnel entrance; this point differs from the evacuation-height CO point in Table 15, and their values are not directly matched.

Table 15. CO responses at different extraction rates without a water curtain.

Number	Extraction Rate (m^3/s)	Exhaust Outlet CO Concentration/ppm	Mean CO Concentration at 1.6 m Height/ppm
1	5	789	65
2	10	920	49
3	15	1124	32
4	20	1005	52
5	25	856	89
6	30	692	128

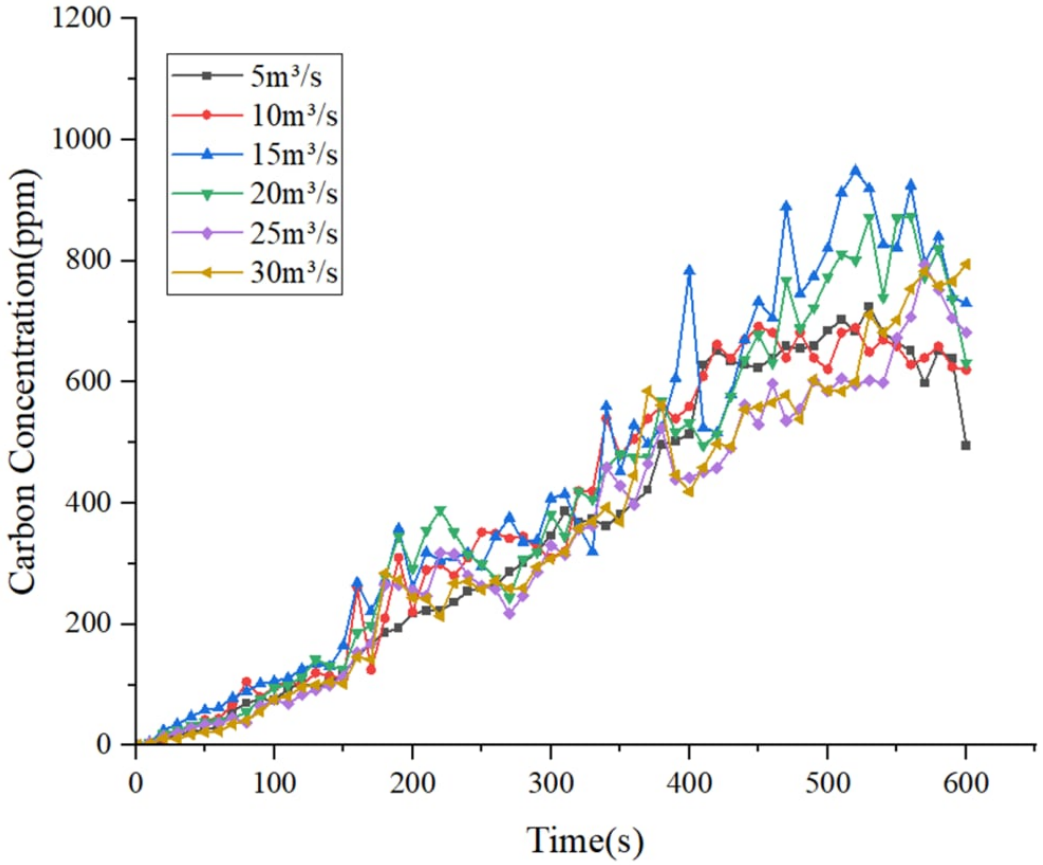


Figure 17. CO concentration time histories at a separate tunnel entrance monitoring point for different extraction rates.

Exhaust vent CO first increases and then decreases with extraction rate (Figure 18 and Table 15). When the rate increases from 15 to 20 m^3/s, exhaust vent CO decreases from 1124 to 1005 ppm, while evacuation-height CO and temperature increase; 15–20 m^3/s is therefore identified as the performance transition interval bounded by adjacent discrete cases.

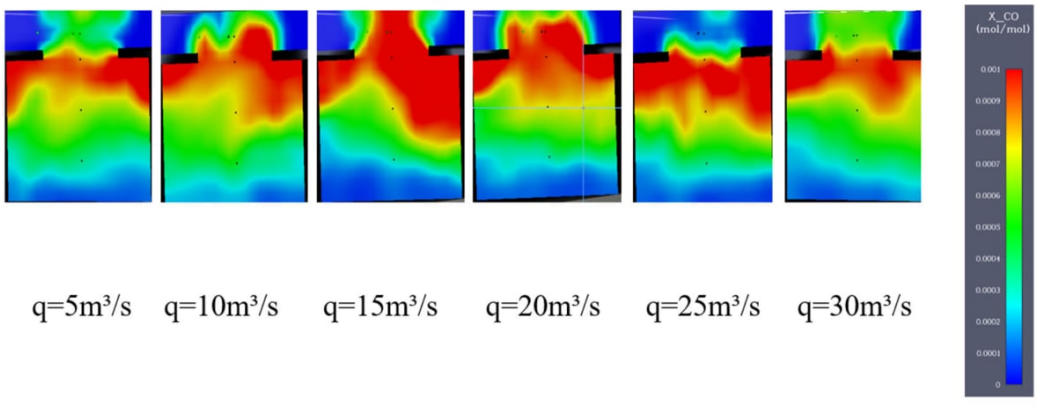


Figure 18. CO mole fraction distributions at the exhaust vent. Note: The color scale X_CO denotes the CO mole fraction in mol/mol; multiplication by 10^6 gives the corresponding value in ppm.

3.1.3. Local Flow Field and Smoke Layer Responses

Figure 19 presents the longitudinal velocity component (U-VEL) near the exhaust vent under near-critical longitudinal ventilation to compare local flow structures. For extraction rates above 15 m^3/s, changes in cross-sectional nonuniformity and local regions of low longitudinal velocity accompany the transition in macroscopic indicators.

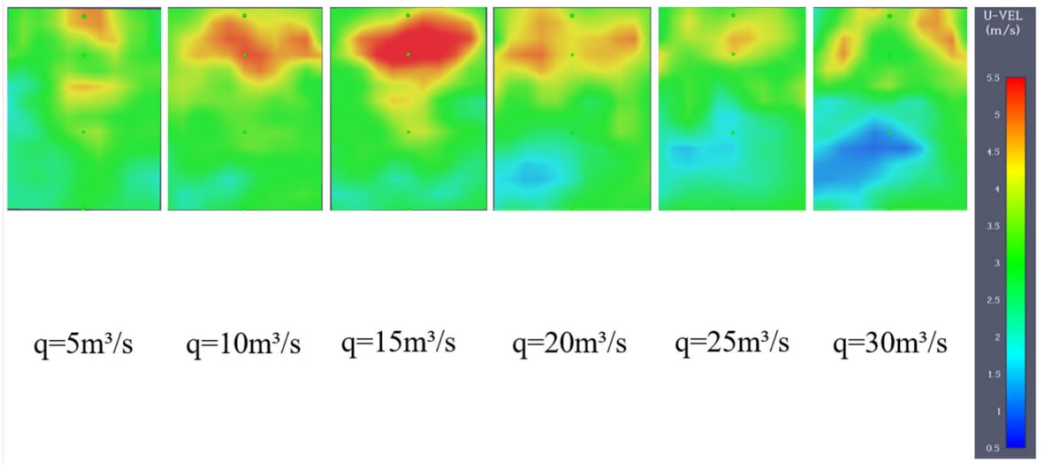


Figure 19. Longitudinal velocity distributions near the exhaust vent for cases without a water curtain. Note: The color scale U-VEL denotes the longitudinal velocity component in m/s, rather than the velocity normal to the exhaust vent.

3.1.4. Species Mass Transport

Table 16 lists the 300–600 s mean results. The non-PRODUCTS mass flow fraction serves as a relative indicator of the mixing state and differs from an independently measured cool air fraction or a plug-holing criterion.

Table 16. Species mass transport at the exhaust vent for cases without a water curtain.

Extraction Rate/$m^3 \cdot s^{-1}$	Total Gas Mass Flow Rate/$kg \cdot s^{-1}$	Combustion Product Mass Flow Rate/$kg \cdot s^{-1}$	Air Mass Flow Fraction/%	Exhaust Vent CO/ppm
15	12.6	10.2	19.0	1124
20	18.0	12.0	33.3	1005
25	24.0	12.5	47.9	856
30	30.6	12.7	58.5	692

When the extraction rate increases from 15 to 30 m^3/s, the total mass flow rate increases from 12.6 to 30.6 kg/s, while the PRODUCTS mass flow rate increases from 10.2 to 12.7 kg/s with progressively smaller increments (Table 16). The non-PRODUCTS mass flow fraction rises from 19.0% to 58.5%, which, together with the decrease in exhaust vent CO, indicates a change in the composition of the extracted airflow.

3.2. Combined Smoke Control Performance of the Water Curtain and Centralized Extraction

3.2.1. Effects of Droplet Size

At the consistent precision of one decimal place used in the table, the temperatures measured 2 m downstream of the water curtain at 1.6 m height are 151.4, 91.6, 76.3, 53.0, and 61.4 °C, respectively. The 500 μm case has the lowest value, approximately 65.0% below the case without a water curtain and 13.7% below the 800 μm case. The maximum ceiling temperature continues to decrease with increasing droplet size, showing that the relative preferences differ among indicators.The results are listed in Table 17 and Figure 20.

Table 17. Macroscopic temperature and CO responses for different droplet sizes.

Droplet Size/μm	No Water Curtain	200	300	500	800
Mean Temperature 2 m Downstream of the Water Curtain at 1.6 m Height/°C	151.4	91.6	76.3	53.0	61.4
Exhaust Vent CO Concentration/ppm	1124	1233	1295	1356	1368
Maximum Ceiling Temperature/°C	608.5	597.6	588.0	559.6	541.0

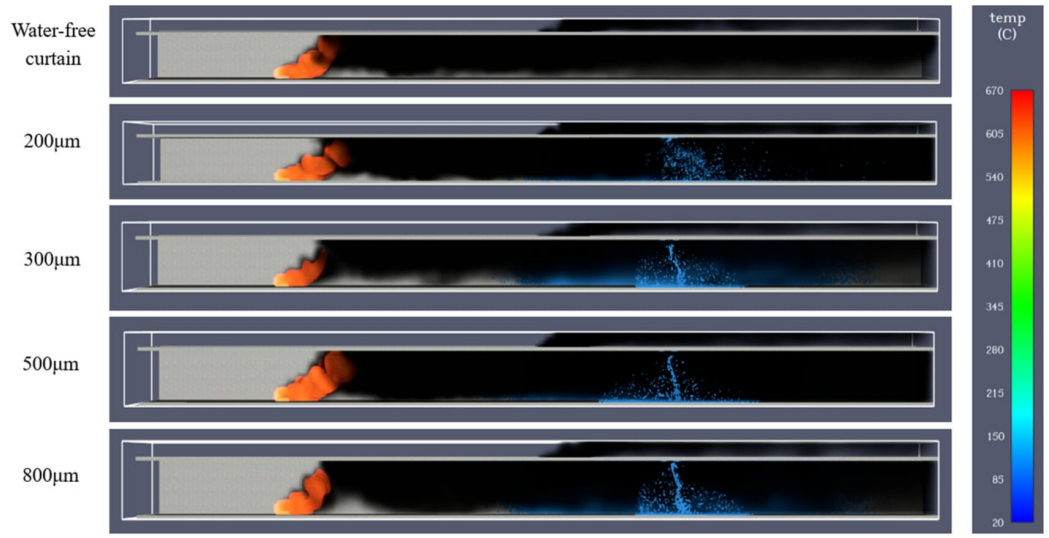


Figure 20. Temperature distributions for different droplet sizes.

3.2.2. Temperature Response

With the baseline water curtain, the maximum ceiling temperature decreases from 559.6 to 542.8 °C as the extraction rate increases from 15 to 18 m^3/s and decreases further to 539.5 °C at 20 m^3/s (Figure 21 and Table 18). The latter decrease is 3.3 °C, indicating a smaller improvement in this temperature indicator.

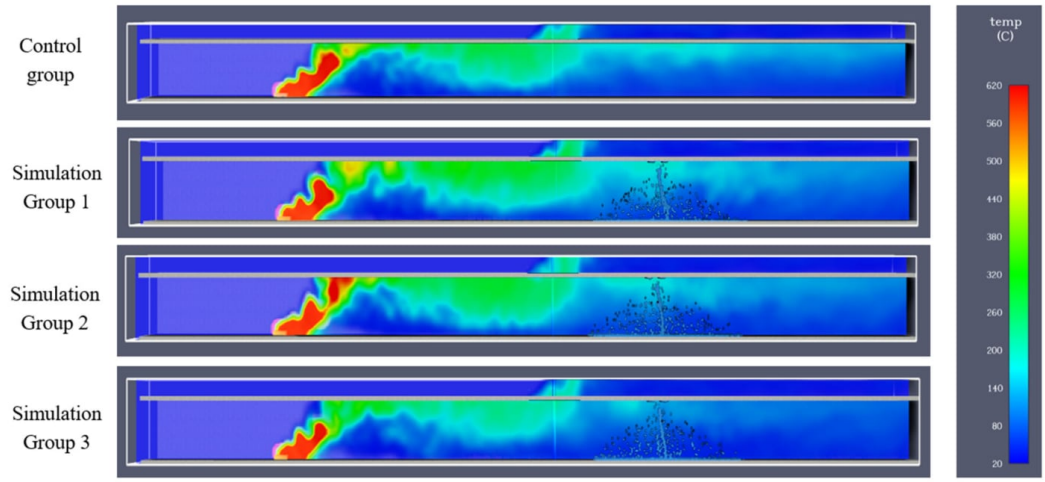


Figure 21. Temperature distributions at different extraction rates with the baseline water curtain.

Table 18. Maximum ceiling temperatures at different extraction rates with the baseline water curtain.

Number	Simulation Type	Extraction Rate/m^3/s	Maximum Ceiling Temperature/°C
1	Control group	15	608.5
2	Simulation group 1	15	559.6
3	Simulation group 2	18	542.8
4	Simulation group 3	20	539.5

3.2.3. CO Concentration and Pollutant Transport Responses

At the same extraction rate of 15 m^3/s, introducing the water curtain increases exhaust vent CO from 1124 to 1356 ppm and decreases evacuation-height CO from 32 to 28 ppm. When the extraction rate in the coupled cases increases from 18 to 20 m^3/s, exhaust vent CO decreases from 1433 to 1411 ppm and evacuation-height CO increases from 20 to 25 ppm (Figure 22 and Table 19), while the maximum ceiling temperature continues to decrease slightly.

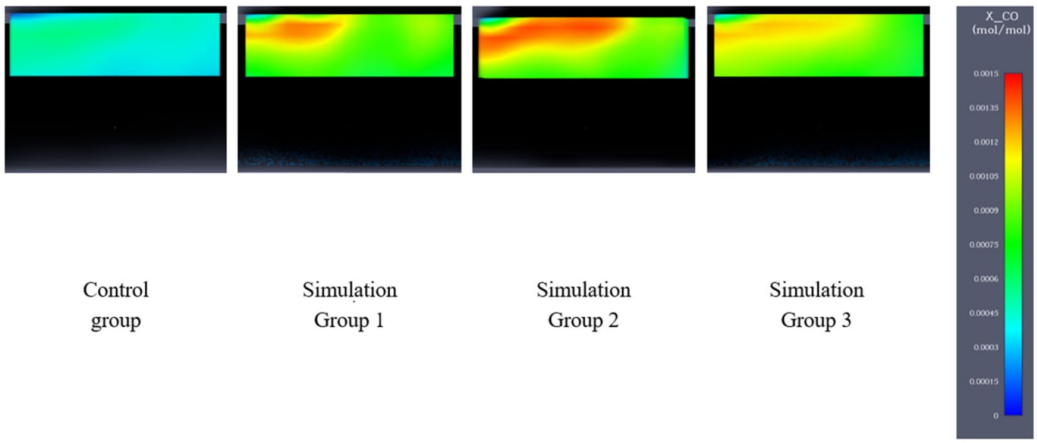


Figure 22. CO mole fraction distributions at the exhaust vent for coupled cases. Note: The color scale X_CO denotes the CO mole fraction in mol/mol; the case groups are defined in Table 13.

Table 19. CO responses at different extraction rates with the baseline water curtain.

Number	Simulation Type	Extraction Rate/m^3/s	Exhaust Vent CO Concentration/ppm	Mean CO Concentration at 1.6 m Height/ppm
1	Control group	15	1124	32
2	Simulation group 1	15	1356	28
3	Simulation group 2	18	1433	20
4	Simulation group 3	20	1411	25

3.2.4. Local Longitudinal Flow Under Coupled Conditions

Figure 23 compares local longitudinal velocity distributions under coupled water curtain conditions, showing pronounced local flow nonuniformity in the 20 m^3/s case. This component differs from the suction velocity normal to the exhaust vent, and its spatial variation provides supporting explanations for relative flow responses among cases.

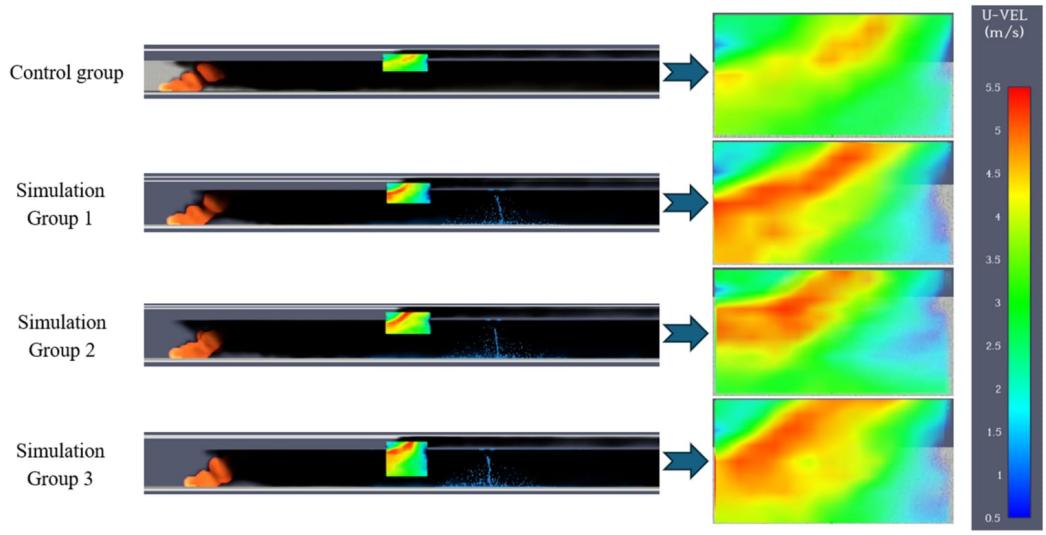


Figure 23. Longitudinal velocity distributions near the exhaust vent for coupled cases. Note: The color scale U-VEL denotes the longitudinal velocity component in m/s; the case groups are defined in Table 13.

3.3. Dimensionless Relationship of Performance Transition Intervals

3.3.1. Transition Intervals at Different Water Curtain Flow Rates

Table 20 accordingly reports intervals bounded by adjacent candidate points, with an interval of 18–19 m^3/s for the baseline 40 L/min case. This 1 m^3/s interval comes from the refined parameter set described in Section 2.6.3; the cases at 15, 18, and 20 m^3/s in Section 3.2 provide a coarser comparison.

As shown in Table 20 and Figure 24, when the flow rate per nozzle increases from 30 to 60 L/min, the smoke extraction performance transition interval gradually shifts from 17–18 to 20–21 m^3/s in a stepwise manner. Adjacent water curtain flow rates may correspond to the same transition interval.

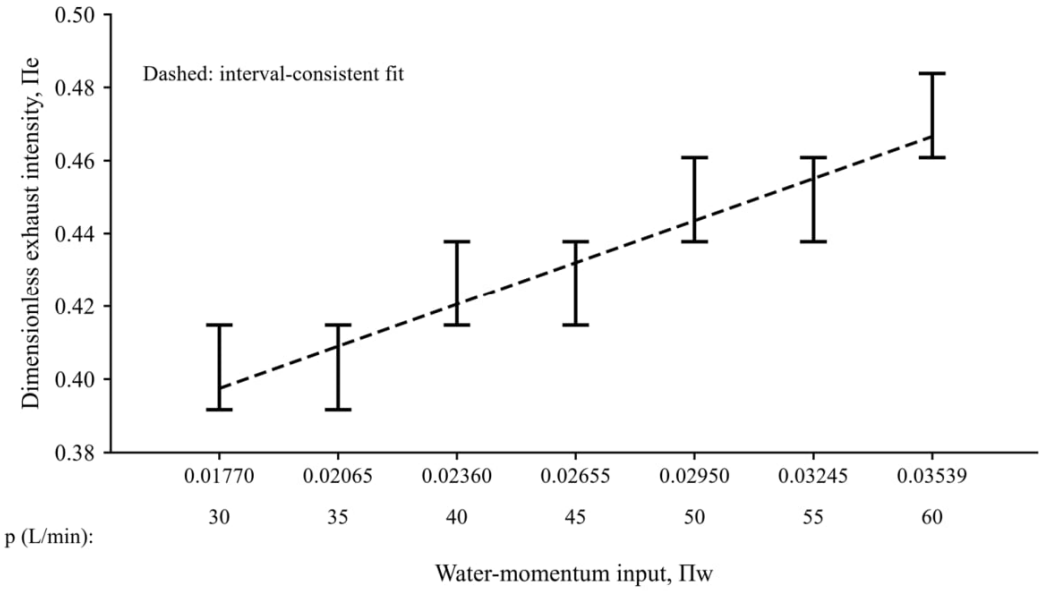


Figure 24. Relationship between the water curtain momentum parameter and the smoke extraction performance transition interval. Note: Interval segments represent ranges bounded by adjacent discrete cases rather than statistical confidence intervals; the dashed line is the interval-constrained linear expression.

Table 20. Smoke extraction performance transition intervals and dimensionless expressions at different water curtain flow rates.

Number	Flow Rate per Nozzle p/(L/min)	Π_w	Extraction Transition Interval/(m^3/s)	Π_e Transition Interval
1	30	0.01770	17–18	0.39171–0.41475
2	35	0.02065	17–18	0.39171–0.41475
3	40	0.02360	18–19	0.41475–0.43779
4	45	0.02655	18–19	0.41475–0.43779
5	50	0.02950	19–20	0.43779–0.46083
6	55	0.03245	19–20	0.43779–0.46083
7	60	0.03539	20–21	0.46083–0.48388

3.3.2. Interval-Constrained Linear Relation

The interval-constrained analysis gives

$$\Pi e = 3.90596 \Pi w + 0.32834 \quad (11)$$

The linear values calculated using Equation (11) fall within all seven reported discrete intervals, with a minimum interval margin of approximately 0.00576.

4. Discussion

4.1. Interpretation of Extraction Performance Transitions

The temperature field and CO concentration results above show that, as the extraction rate increases, smoke control performance at evacuation height first improves and then deteriorates.

High extraction rates may enhance entrainment of the air below, while the correspondence between this flow behavior and the macroscopic performance transition requires assessment using the individual indicators.

The decrease in exhaust vent CO may be associated with airflow dilution, but concentration itself differs from the combustion product mass flow rate or effective smoke extraction efficiency; the flow field and species transport results provide supporting explanations.

The species mass transport results in Table 16 support the interpretation of increased dilution and entrainment at high extraction rates; they do not indicate a decrease in combustion product removal.

The longitudinal velocity shown in Figure 19 differs from the suction velocity normal to the exhaust vent; for a specified exhaust vent area and nominal volumetric extraction rate, the area-averaged normal velocity still increases with extraction rate. This contour plot alone does not determine the onset of plug-holing.

The temperature response in Table 14 and Figure 16 identifies a discrete transition range in the temperature response but does not independently determine the onset of plug-holing.

In cases without a water curtain, temperature and evacuation-height CO show comparatively favorable combined performance at 15 m^3/s and increase in the next adjacent case at 20 m^3/s; the interval of 15–20 m^3/s is therefore reported rather than a precise critical value. Plug-holing may affect these indicators by penetrating the smoke layer and entraining air from below, but its location, timing, and local criteria differ from this macroscopic discrete interval. The onset conditions of plug-holing were not determined individually in this study.

4.2. Water Curtain Parameter Matching and Competing Responses

Based on the droplet-size comparison in Section 3.2.1 and 500 μm serves as a representative droplet size when cooling at evacuation height is prioritized in this study and

does not represent a common optimum for all temperature and smoke control indicators. Differences among droplet sizes in cooling location, droplet transport by airflow, and vertical penetration may affect these responses, while the present outputs do not quantitatively separate the contributions of evaporative cooling and droplet momentum drag; further analysis requires gas–liquid energy, momentum, and species flux budgets.

Since the baseline water curtain case at 20 m^3/s still corresponds to a lower maximum ceiling temperature, these results alone do not establish 18 m^3/s as a common optimum for all indicators; a combined assessment with the CO response is required.

Thus, 18 m^3/s is a representative value with comparatively favorable CO indicators in this set of cases, reflecting a trade-off between temperature and pollutant indicators. A budget analysis that quantitatively separates the contributions of evaporative cooling and droplet momentum drag has not been established; the two are interpreted as mechanisms that may act together.

Without a water curtain, the change from 15 to 20 m^3/s is accompanied by increases in temperature and evacuation-height CO, corresponding to the 15–20 m^3/s interval. With the baseline water curtain, the change from 18 to 20 m^3/s increases evacuation-height CO while ceiling temperature still decreases slightly, indicating a trade-off among indicators rather than a common optimum for all indicators.

4.3. Validation Scope and Assessment Coverage

The T2-2 data examine the baseline ceiling temperature field of a longitudinally ventilated fire and do not include the combined ceiling centralized smoke extraction and water curtain configuration used in this study. An independent full-scale experimental benchmark directly matching this coupled configuration was not obtained. Section 2.5.3 examines the macroscopic temperature and CO responses under coupled conditions by comparing 1:10 reduced-scale experiments with same-scale FDS simulations; the resulting validation is not equivalent to independent full-scale validation of the prototype coupled system.

Reduced-scale validation does not cover all parameter combinations; mesh and particle release rate sensitivities also concern time-averaged outputs, while convergence of instantaneous droplet trajectories and microscale gas–liquid exchange remains unverified.

The local mesh sensitivity analysis in Section 2.4.2 concerns the time-averaged longitudinal velocity and CO outputs for the tested case; it does not establish mesh convergence of instantaneous droplet trajectories, local entrainment details, or microscale gas–liquid momentum and heat transfer processes.

Computational particle release rate sensitivity shows small variations in the tested time-averaged macroscopic outputs. It does not replace experimental validation or establish convergence of instantaneous individual droplet trajectories or microscale gas–liquid momentum and heat exchange.

Local mesh sensitivity covers the representative coupled case at 18 m^3/s, with the remaining extraction rates not tested individually; the local flow-field results therefore do not independently identify plug-holing or quantify gas–liquid momentum exchange.

Visibility, thermal dose, and fractional effective dose (FED) are not evaluated in this study; the temperature and CO indicators therefore provide a partial assessment of occupant tenability.

4.4. Applicability of the Dimensionless Relation

Equation (11) shows in-sample interval consistency; independent external testing has not been performed, and the relation does not predict a precise critical extraction rate or a continuous optimum. Accordingly, the coefficient of determination R^2 is not used to express

its predictive accuracy as a point-value regression model. The applicable conditions are specified below.

The interval width reflects the sampling resolution rather than a statistical confidence interval and does not give a precise optimum extraction rate within the interval or a universal plug-holing threshold.

The assessment remains within fixed fire size, tunnel cross-section, and exhaust vent arrangement conditions. Accordingly, the results identify performance transition characteristics under the present conditions and are not directly generalized as a universal critical extraction rate for plug-holing.

Equation (11) summarizes the in-sample relationship between water curtain input and the smoke extraction performance transition interval under fixed conditions. Its scope is a 100 m × 4 m × 3 m tunnel, an 8 MW fire, a near-critical longitudinal velocity of 2.0 m/s, an 8 m^2 exhaust vent, a water curtain 8 m downstream of the vent, three downward-facing nozzles, a volume median diameter of 500 μm, an initial velocity of 5 m/s, and a flow rate of 30–60 L/min per nozzle; the spray angle and droplet size distribution remain as specified in Table 4. The relation is not for direct extrapolation to fan control settings, critical plug-holing values, or engineering design formulas for actual tunnels.

Froude similarity mainly constrains gas-phase buoyancy and inertia. With the same working fluids, the Froude criterion alone at a single geometric scale does not simultaneously ensure similarity in droplet Reynolds number, Weber number, the ratio of evaporation time to gas-phase transport time, spray breakup, heat transfer, and the spatial flow distribution. Thus, achieving the reduced-scale design flow rate does not imply complete similarity of the microscopic water curtain processes. The present 1:10 experiments support the macroscopic temperature and CO responses under the actual reduced-scale spray conditions; cross-scale application of Equation (11) requires independent validation. Fire size, cross-section, blockage, wall heat transfer, and the coupled pressure–flow behavior of actual nozzles may all alter the present relation.

5. Conclusions

Under a fixed 8 MW fire and near-critical longitudinal ventilation, this study combines FDS simulations, 1:10 Froude-scaled experiments, and dimensionless analysis to investigate the performance transition of centralized smoke extraction and the parameter responses after introducing a water curtain. The main conclusions are as follows.

(1) Comparisons between reduced-scale experiments and same-scale FDS simulations provide validation evidence for macroscopic temperature and CO responses; the T2-2 full-scale data validate the baseline temperature field under longitudinal ventilation. An independent full-scale validation benchmark for combined centralized smoke extraction and water curtain operation was not obtained in this study.

(2) In a 100 m × 4 m × 3 m tunnel with an 8 MW fire and a longitudinal velocity of 2.0 m/s, temperature and evacuation-height CO improve when the extraction rate without a water curtain increases from 5 to 15 m^3/s and then increase in the 20 m^3/s case. The rate of 15 m^3/s is a representative suitable value among the discrete cases, and 15–20 m^3/s is the performance transition interval, whose meaning differs from a universal plug-holing threshold.

(3) With the baseline water curtain, 18 m^3/s corresponds to comparatively low evacuation-height CO in this set of cases, while 20 m^3/s still produces a slightly lower maximum ceiling temperature; the former therefore reflects a trade-off among indicators. In the refined parameter set, increasing the flow rate per nozzle from 30 to 60 L/min shifts the smoke extraction performance transition interval from 17–18 to 20–21 m^3/s. Evaporative cooling and droplet momentum drag may jointly affect these responses, and their contributions have not been quantitatively separated.

(4) For flow rates of 30–60 L/min per nozzle, this study defines $\prod_e = \frac{Q_e}{A_e\sqrt{gH}}$ and $\prod_w = \frac{\rho_w Q_w V_d}{\rho_a g H A_t}$, and the constrained expression for the seven discrete intervals is $\Pi_e = 3.90596\Pi_w + 0.32834$. This equation describes the sample relationship under the conditions specified in Section 4.4 and within $\Pi_w = 0.01770$–0.03539; independent cross-scale testing has not been performed, and the equation is not for direct use in engineering design.

(5) Mesh and computational particle release rate sensitivities support the numerical stability of the tested time-averaged macroscopic outputs; convergence of instantaneous droplet trajectories and microscale gas–liquid exchange remains unverified. Froude scaling also does not ensure complete similarity of microscopic spray processes; extension to engineering applications requires a wider range of scales and operating conditions and independent validation.

Author Contributions: X.Z. (Xiaokun Zhao) was responsible for conceptualization and theoretical analysis; Y.T. was responsible for experiments, data recording and analysis, and manuscript writing; X.Z. (Xiangzhong Zhang) and A.S. were responsible for data checking and validation; W.W. and D.Y. were responsible for manuscript organization and error correction. All authors have read and agreed to the published version of the manuscript.

Funding: This research was funded by the National Natural Science Foundation of China (grant number 52464018), the Shanxi Provincial Key Research and Development Program (grant number 202304290000002), the 2023 Science and Technology Innovation Program for Higher Education Institutions in Shanxi Province (grant number 2023L285), and the 2025 Shanxi Datong University Postgraduate Academic and Practical Innovation Project (grant number 25SJCX17).

Institutional Review Board Statement: Not applicable.

Informed Consent Statement: Not applicable.

Data Availability Statement: Data and other information can be obtained by contacting 18215363492@163.com.

Conflicts of Interest: The authors declare no conflicts of interest.

References

1. Liu, Y. Study on Smoke Flow Characteristics and Efficient Control Methods for Road Tunnel Fires under Centralized Smoke Extraction. Ph.D. Thesis, Chongqing University, Chongqing, China, 2023.
2. Hu, L.H.; Zhou, J.W.; Huo, R.; Peng, W.; Wang, H. Confinement of Fire-Induced Smoke and Carbon Monoxide Transportation by Air Curtain in Channels. *J. Hazard. Mater.* **2008**, *156*, 327–334. [CrossRef] [PubMed]
3. Oka, Y.; Atkinson, G.T. Control of Smoke Flow in Tunnel Fires. *Fire Saf. J.* **1995**, *25*, 305–322. [CrossRef]
4. Liu, Y.; Yang, D. Experimental Study on Synergistic Effect of Exhaust Vent Layout and Exhaust Rate on Performance of Ceiling Central Smoke Extraction in Road Tunnel Fires. *Int. J. Therm. Sci.* **2023**, *183*, 107886. [CrossRef]
5. Ingason, H.; Li, Y.Z. Model Scale Tunnel Fire Tests with Point Extraction Ventilation. *J. Fire Prot. Eng.* **2011**, *21*, 5–36. [CrossRef]
6. Chen, C.F.; Shu, C.M.; Ho, S.P.; Kung, H.C.; Chien, S.W. Effects of Ventilation and Water Spray in a Model-Scale Tunnel Fire. *Fire Technol.* **2018**, *54*, 75–96. [CrossRef]
7. Zhu, H.; Du, W.; Li, W. Experimental Study on the Influence of High-Pressure Water Mist on the Ceiling Temperature of a Longitudinally Ventilated Tunnel. *Fire* **2024**, *7*, 262. [CrossRef]
8. Li, Y.Z.; Lei, B.; Ingason, H. Study of Critical Velocity and Backlayering Length in Longitudinally Ventilated Tunnel Fires. *Fire Saf. J.* **2010**, *45*, 361–370. [CrossRef]
9. Li, Y.Z.; Lei, B.; Ingason, H. The Maximum Temperature of Buoyancy-Driven Smoke Flow beneath the Ceiling in Tunnel Fires. *Fire Saf. J.* **2011**, *46*, 204–210. [CrossRef]
10. Chen, T.B.Y.; Yuen, A.C.Y.; Cordeiro, I.M.D.C.; Liu, H.; Cao, R.; Ellison, A.; Yeoh, G.H. In-Depth Assessment of Cross-Passage Critical Velocity for Smoke Control in Large-Scale Railway Tunnel Fires. *Fire* **2022**, *5*, 140. [CrossRef]
11. Tanaka, F.; Majima, S.; Kato, M.; Kawabata, N. Performance Validation of a Hybrid Ventilation Strategy Comprising Longitudinal and Point Ventilation by a Fire Experiment Using a Model-Scale Tunnel. *Fire Saf. J.* **2015**, *71*, 287–298. [CrossRef]
12. Chen, L.F.; Hu, L.H.; Tang, W.; Yi, L. Studies on Buoyancy Driven Two-Directional Smoke Flow Layering Length with Combination of Point Extraction and Longitudinal Ventilation in Tunnel Fires. *Fire Saf. J.* **2013**, *59*, 94–101. [CrossRef]

13. Wang, Q.; Guo, F.; Yao, Y.; Zhang, X. Numerical Study on Plug-Holing of Double Fires in Tunnel with Centralized Smoke Exhaust. *Tunn. Undergr. Space Technol.* **2023**, *142*, 105419. [CrossRef]
14. Li, Y.; Huang, F.; Ma, C.; Tang, K. A Simulation Study on the Smoke Control Effect with Different Smoke Exhaust Patterns and Longitudinal Air Supply for Ultra-Wide Tunnels. *Fire* **2022**, *5*, 72. [CrossRef]
15. Liu, Q.; Xu, Z.; Xu, W.; Tagne, S.M.S.; Tao, H.; Zhao, J.; Ying, H. Study of the Heat Exhaust Coefficient of Lateral Smoke Exhaust in Tunnel Fires: The Effect of Tunnel Width and Transverse Position of the Fire Source. *Fire* **2022**, *5*, 167. [CrossRef]
16. Shi, Y.; Qian, S.; Zhao, P.; Guo, P.; Gao, Z. Influence of Smoke Exhaust Volume and Smoke Vent Layout on the Ceiling Centralized Smoke Exhaust Effect in Tunnel Fires. *Fire* **2024**, *7*, 78. [CrossRef]
17. Wang, J.; Huang, D.; Kong, X.; Jiang, X.; Lu, K. Water Spray Effects on Fire Smoke Stratification in a Symmetrical V-Shaped Tunnel. *Fire Technol.* **2025**, *61*, 999–1021. [CrossRef]
18. Nishino, R.; Ren, N.; Noda, Y.; Tanaka, F. Large Eddy Simulation of Smoke Blocking by Water Sprays in a Tunnel Fire. *Tunn. Undergr. Space Technol.* **2022**, *121*, 104278. [CrossRef]
19. Farrell, K.; Hassan, K.; Hossain, D.; Ahmed, B.; Rahnamayiezekavat, P.; Douglas, G.; Saha, S. Water Mist Fire Suppression Systems for Building and Industrial Applications: Issues and Challenges. *Fire* **2023**, *6*, 40. [CrossRef]
20. Yuan, J. Segmented Tunnel Smoke-Exhaust System and Method Using Water-Curtain Isolation. Chinese Patent ZL201010028981.2, 16 June 2010.
21. Yao, Y.; Wang, Y.; Chen, L.; Ren, F.; Shi, C. Numerical Study on Coupled Smoke Control Using Longitudinal Ventilation and Naturally Ventilated Shafts during Fires in a Road Tunnel. *Fire* **2023**, *6*, 126. [CrossRef]
22. *JTG/T D70/2-02—2014*; Guidelines for Design of Ventilation of Highway Tunnels. China Communications Press: Beijing, China, 2014.
23. *GB 50016—2014*; Code for Fire Protection Design of Buildings. China Planning Press: Beijing, China, 2014.
24. *DG/TJ 08-2033—2017*; Standard for Design of Road Tunnels. Tongji University Press: Shanghai, China, 2017.
25. *CJJ 221—2015*; Code for Design of Urban Underground Road Engineering. China Architecture & Building Press: Beijing, China, 2015.
26. *JTG 3370.1—2018*; Specifications for Design of Highway Tunnels Volume 1 Civil Engineering. China Communications Press: Beijing, China, 2018.
27. *GB 55036—2022*; General Code for Fire Protection Facilities. China Planning Press: Beijing, China, 2022.
28. *GB 50084—2017*; Code for Design of Sprinkler Systems. China Planning Press: Beijing, China, 2017.
29. PIARC. *Design Fire Characteristics for Road Tunnels*; Report 2017R01EN; PIARC Technical Committee 3.3 Road Tunnel Operations: Paris, France, 2017; ISBN 978-2-84060-471-6.
30. Hamins, A.; Maranghides, A.; Mulholland, G.W. *The Global Combustion Behavior of 1 MW to 3 MW Hydrocarbon Spray Fires Burning in an Open Environment*; NISTIR 7013; National Institute of Standards and Technology: Gaithersburg, MD, USA, 2003. [CrossRef]
31. McGrattan, K.; Hostikka, S.; McDermott, R.; Floyd, J.; Vanella, M. *Fire Dynamics Simulator User's Guide*, 6th ed.; NIST Special Publication 1019; National Institute of Standards and Technology: Gaithersburg, MD, USA, 2013. Available online: https://tsapps.nist.gov/publication/get_pdf.cfm?pub_id=913619 (accessed on 29 October 2026).
32. Wu, Y.; Bakar, M.Z.A. Control of Smoke Flow in Tunnel Fires Using Longitudinal Ventilation Systems: A Study of the Critical Velocity. *Fire Saf. J.* **2000**, *35*, 363–390. [CrossRef]
33. McGrattan, K.; McDermott, R.; Vanella, M.; Hostikka, S.; Floyd, J. *Fire Dynamics Simulator Technical Reference Guide, Volume 1: Mathematical Model*, 6th ed.; NIST Special Publication 1018-1; National Institute of Standards and Technology: Gaithersburg, MD, USA, 2000. Available online: https://nvlpubs.nist.gov/nistpubs/SpecialPublications/NIST.SP.1018e6.pdf (accessed on 29 October 2026).

Disclaimer/Publisher's Note: The statements, opinions and data contained in all publications are solely those of the individual author(s) and contributor(s) and not of MDPI and/or the editor(s). MDPI and/or the editor(s) disclaim responsibility for any injury to people or property resulting from any ideas, methods, instructions or products referred to in the content.